# Stresses in Oxidized Claddings and Mechanical Stability of Oxide Scales

**H. Steiner, J. Konys**
**Institut für Materialforschung**
**Programm Nukleare Sicherheitsforschung**

**März 2006**

# Stresses in oxidized claddings and mechanical stability of oxide scales

H. Steiner, J. Konys

Institut für Materialforschung

Programm Nukleare Sicherheitsforschung

# Spannungen in oxidierten Hüllrohren und mechanische Stabilität von Oxidschichten

## Zusammenfassung

In einem Beschleuniger getriebenen System ist die Existenz von Oxidschichten auf metallischen Komponenten von großer Bedeutung für deren Standzeit, da sie den Lösungsangriff durch das Flüssigmetall verhindern können. Deshalb muss die mechanische Langzeit-Stabilität von schützenden Oxidschichten erforscht werden. Sowohl Spannungen aufgrund von Temperaturwechseln als auch Wachstumsspannungen können eine Gefahr für die Oxidschichten darstellen. Folglich wurden Modelle zu deren Berechnung in Duplex-Schichten entwickelt und angewendet. Im Falle eines reinen Druckspannungszustandes liefert die elastische Spannungsenergie vermutlich ein brauchbares Kriterium für die Vorhersage des mechanischen Versagens der Oxidschicht. Im Falle eines gemischten Spannungszustands (Zugspannungs- und Druckspannungs-Komponenten) ist ein solch einfaches Kriterium möglicherweise nicht ausreichend.

Experimentelle Beobachtungen zum mechanischen Versagen von Oxidschichten werden diskutiert, und zwar sowohl für Oxidschichten, die unter Gasatmosphäre, als auch für Oxidschichten, die im Flüssigmetall entstanden sind. Diese liefern uns Hinweise zum Schadensmechanismus und zum Spannungszustand. Eine wichtige Frage, die gelöst werden muss, betrifft die nach der Ursache des mechanischen Versagens, ob es nämlich allein durch Temperaturwechsel hervorgerufen wir oder ob es auch bei konstanter Temperatur durch Wachstumsspannungen verursacht werden kann.

## Abstract

The presence of oxide scales on metallic components in an accelerator driven system is very important for their endurance, as they might prevent dissolution attack by the heavy liquid metal. The long-term mechanical stability of protective oxide scales must be investigated. Stresses due to temperature changes and also growth stresses may pose a significant threat to the integrity of the oxide scales. For this aim models for the stresses arising in duplex scales have been developed and applied. In case of a compressive stress state the elastic strain energy in the oxide scale may suffice to judge on the onset of mechanical failures. But this may not be true in case of a mixed stress state (tensile and compressive components).

Observations on mechanical failures of oxide scales grown under gas atmospheres and in heavy liquid environments are discussed. They provide us information on the failure mechanisms and hints on the stress state leading to failure. An important question, which must be clarified, is whether the mechanical failures are only caused by temperature changes or whether some of them have also occurred at steady-state due to growth stresses.

**Table of Contents**                                                        Page

# 1.    Introduction

The oxide scales growing on metal components exposed to high temperature environments like gas atmospheres or heavy liquid metals act as diffusion barriers and protect the metal from rapid degradation or dissolutuion. For example, it is known that in heavy liquid metal environments dissolution rates of unprotected steel components are by order of magnitude higher than the dissolution rates of oxide scales.

Optimum resistance to oxidation arises when the protective oxide layer remains adherent and mechanically intact so that continued reaction arises through solid-state diffusion [1]. Iron oxide scales are brittle under the temperatures foreseen for heavy liquid metal loops in accelerator driven systems. Therefore stresses may impair the mechanical integrity of the oxide scales and are of great importance as they can lead to cracking and debonding or spalling of oxide scales. The renewed oxidation after spalling may lead to enhanced oxidation rates but to less protective scales, as alloying elements like Cr may eventually not be able to contribute to the renewed oxidation process due to depletion effects.

There are different sources of stresses in the oxide scales, the most important ones are growth stresses (geometrically-induced and intrinsic) and thermal stresses. In a first step, we will describe the action of these stresses separately but in a second step we have to investigate their combined effect. In a third step we have to find and apply criteria for the failure of the oxide scales.

Depending on the temperature, the oxygen partial pressure and the content of minor alloying elements like Cr or Al single layer or multi-layer oxide scales may be formed. In this report we are mainly considering the behaviour of oxide scales on austenitic and martensitic steels. For these steels either a single layer Fe/Cr spinel scale is formed or a duplex scale consisting of a magnetite subscale in the outer part and a Fe/Cr spinel subscale in the inner part, depending strongly on the temperature, the Cr content and the oxygen partial pressure. In this report we are considering the duplex layer case, as it encompasses the single spinel layer case.

Our main interest is with oxide scales in a heavy liquid environment, but we will also discuss the experience gained for oxide scales grown under gas atmospheres. The stress levels should mainly depend on the oxide scale thickness and on the temperature changes and temperature gradients. But the environment could influence some mechanical properties like fracture toughness and surface energies and of course growth of cavities.

# 2.    Theoretical background

This work is meant to investigate the situation for metallic components in the test loop CORRIDA. As the maximum temperature in this loop is 550°C, we have no important effects of plastic flow or creep relaxation in the oxide scales. For thin oxide scales and thick metallic substrates the stresses in the metal phase are at least one order of magnitude lower than in the oxide scale and are therefore far below the elastic limit.
It should be noted that we consider in the following cylindrical test specimens and are therefore concerned with elastic stress solutions in a cylindrical coordinate system.

The elastic stress solutions are then used to calculate the elastic strain energy for the assessment of mechanical stability of the oxide scales.

## 2.1    Stresses due to temperature changes

Stresses develop in both oxide scale and metallic substrate during temperature changes as a result of a mismatch between the thermal expansion coefficients of the oxide scale $\alpha_{ox}$ and the metal substrate $\alpha_{me}$. Austenitic, ferritic, and martensitic steels have different values for the thermal expansion coefficients and it is interesting to evaluate their performance under temperature changes. Also, we have to look into the problem of duplex scales as magnetite and Fe/Cr spinel differ in their expansion coefficients. We consider duplex scale formation as a sort of standard case, although it is known that, on martensitic steels [2] and also on austenitic steels [3] single layer Fe/Cr spinel scales may be formed depending on the temperature, the Cr content of the steel, and the oxygen content in the heavy liquid metal. In this case the stresses, which are calculated for the spinel layer, would then be relevant.

In the following we consider only isotropic thermal expansion coefficients. This means that the stress state in the specimens will to a first approximation be bi-axial. In case of an-isotropic thermal expansion coefficients the axial stress components could differ considerably from the hoop stresses. In thin-walled tubes the radial stresses are in any case distinctly smaller than the hoop stress and the axial stress. This is not true for a solid cylinder, where the hoop stress and the radial stress are equal.

For an accelerator driven system we have to expect many temperature cycles of different nature during the lifetime of a metallic component, especially if we include safety aspects. But for the time being, we restrict our investigation to situations, which are of greatest interest to us. Namely, we consider a situation typical for test specimens in test loops like CORRIDA with a temperature decrease after a certain period of oxidation at a certain temperature. The temperature prior to the temperature decrease is noted as $T_{ox}$. This situation is considered as a sort of standard case. It is most relevant for heavy liquid metal test loops like CORRIDA.

Our final goal is to assess the propensity for cracking, scale decohesion or even spalling of the oxide scale due to thermal cycling, and for this we must know the stress state in the oxide scale during the whole service lifetime of a test component. The stress state during a temperature ramp is determined by the stress state at the beginning of the ramp and the stress changes arising by the temperature change and eventual stress relaxation effects. The stress state at the beginning of the temperature ramp is a function of the whole temperature history experienced by the metallic component. In a liquid metal loop like CORRIDA one typical situation for a test specimen is that it is oxidized at a certain temperature for a certain time and then unloaded, that means the temperature interval goes down to room temperature. Such a situation is considered as a standard case Thus, in this note we investigate only the stresses due to temperature changes without considering any relaxation effects.

Assuming a bi-axial stress state in the oxide scale and in the metallic substrate, general plane strain and equality of radial displacements at the interface, one can, in

2

case of isothermal conditions for the test specimen, derive the following expression for the mean hoop stress in the oxide scale:

$$\Delta\sigma_{\Theta}^{therm,ox} = \frac{E^{ox}}{1-\nu^{ox}} \cdot \frac{1.}{1 + \frac{\delta^{ox}}{s^{me}} \cdot \frac{E^{ox}}{1-\nu^{ox}} \cdot \frac{1-\nu^{me}}{E^{me}}} \cdot \int_{T_{ox}}^{T} \Delta\alpha(\breve{T}) \cdot d\breve{T} \qquad (1)$$

$$\Delta\alpha(T) = \alpha_{me}(T) - \alpha_{ox}(T) \qquad (2)$$

In case of thin oxide scales on relatively thick metallic substrates, we can use the simplified formula:

$$\Delta\sigma_{\Theta}^{therm,ox} = \frac{E^{ox}}{1-\nu^{ox}} \cdot \int_{T_{ox}}^{T} \Delta a(\breve{T}) \cdot d\breve{T} \qquad (3)$$

The eq. (3) can easily be generalized to multi-layered oxide scales. We have simply to use in eq. (2) the thermal expansion coefficient relevant for the sublayer. For thicker subscales correction factors must be applied which depend on the ratios of the interface radii.

According to our assumption of a bi-axial stress state in the oxide scale we have also:

$$\Delta\sigma_{z}^{therm,ox} = \Delta\sigma_{\Theta}^{therm,ox} \qquad (4)$$

We can calculate the radial stress at the interface of the oxide scale and the metallic substrate with the help of the following relation generally applicable for thin layers:

$$\Delta\sigma_{r}^{int} = -\frac{\delta^{ox}}{r^{int}} \cdot \Delta\sigma_{\Theta}^{ox} \qquad (5)$$

The hoop stress in the metallic substrate can be determined with the help of the force balance:

$$\sum_{i}(\delta_{i}^{ox} \cdot \Delta\sigma_{\Theta,i}^{therm,ox}) + s^{me} \cdot \Delta\sigma_{\Theta}^{therm,me} = 0 \qquad (6)$$

In eq. (6) we have assumed that we have a multi-layered oxide scale.

The thermal expansion coefficients are, in general, functions of the temperature T. Therefore we have applied in eqs. (1) – (3) integrals over the temperature interval between $T_{ox}$ (oxidation temperature) and T. In the literature one often encounters formulas which use averaged values of the thermal expansion coefficients. These averaged values can only be correct for a certain temperature interval. The averaged thermal expansion coefficient in a temperature interval $T_1$, $T_2$ is given by:

$$\alpha^{av}(T_1, T_2) = \frac{1}{T_2 - T_1} \cdot \int_{T_1}^{T_2} \alpha(T) \cdot dT \tag{7}$$

It depends on the values of $T_1$ and $T_2$. In the literature are often given averaged thermal expansion coefficients without noting the values of the temperature interval. It is very dangerous to use such averaged values. The thermal expansion coefficient of certain materials, for example that of steels, can often be approximated by a linear function of the temperature:

$$\alpha(t) = \alpha_0 + \alpha_1 \cdot T \tag{8}$$

In this case the averaged thermal expansion coefficient for the temperature interval between $T_1$ and $T_2$ is given as:

$$\alpha^{av}(T_1, T_2) = \alpha_0 + 1/2 \cdot (T_1 + T_2) \cdot \alpha_1 \tag{9}$$

In case of non-isothermal conditions we can calculate the mean thermal strains in the oxide scale and the metallic substrate by using the respective mean temperatures $T_{av}$:

$$\Delta\varepsilon_{av,T}^{me,ma,sp} = \int_{T_{ox}}^{T_{av}^{me}/T_{av}^{ma}/T_{av}^{sp}} \alpha^{me/ma/sp}(T) dT \tag{10}$$

The state at $T_{ox}$ can to a first approximation be considered as isothermal, but the intermediate states during cool-down can be non-isothermal depending on the cool-down procedure and then the mean temperatures in the oxide subscales and in the metallic substrate will all be different. This also means that radial temperature gradients are present, which lead to thermal stresses. These thermal stresses must be added to the stresses resulting from the change of the mean temperatures. They are compressive on the hot side and tensile on the cold side of the sublayer. The difference between the hot and the cold side can be estimated for a linear temperature distribution with the help of the following formulas:

4

$$\Delta\sigma_{\Theta,lay}^{rad.grad.} = \Delta\sigma_{z,lay}^{rad.grad.} = \frac{E_{lay} \cdot \alpha_{lay}(T_{av}) \cdot \Delta T_{lay}}{1 - \nu_{lay}} \qquad (11)$$

The stress distribution for this simple case of a linear temperature distribution is then given as:

$$\sigma_{\Theta}^{rad.grad.}(t) = \sigma_z^{rad.grad.}(t) = (1/2 - t) \cdot \Delta\sigma_{\Theta,lay}^{rad.grad.} \qquad (12)$$

t = dimensionless distance from the inner radius of the subscale  t= [0,1]

The mean stress in the layer would therefore not be changed by a linear radial temperature gradient.

## 2.2    Growth stresses

Another source of stress is provided by the oxidation process itself. The so-called growth stresses can, in general, consist of a geometrically induced and an intrinsic contribution. The geometrically induced part appears in curved specimens but is zero in flat components. It increases with decreasing radius of curvature of the oxidizing surface and it is due to the component of the oxidation strain tensor, which acts orthogonal to the surface of the component. In case of cylinders this is the radial component of the oxidation strain tensor. The lateral components are in any case much smaller than the orthogonal one. They are responsible for the intrinsic growth stresses. If they are zero we would have, except for end effects, no growth stresses in flat components. Although the lateral components are in any case much smaller than the orthogonal one they can make a considerable contribution to the growth stresses.

The presence of lateral oxidation strain components and their magnitude is still a question of debate and research. For oxide scales on austenitic steels we have found in the literature, which indicate the existence of lateral components. Noden et al [4] have observed axial length increases of thin sections of austenitic steels oxidized in carbon and oxygen bearing gases at 900 $^0$C. At least part of the length increase could be attributed to the oxidation process itself. If the oxidation strain tensor has no axial component, there would be no length increase, except for the effect of the carburization of the steel. Noden et al [4] have found complex multi-layered oxide scales on the steel specimens.

The axial extensions of thin slabs of austenitic steel 20Cr25Ni oxidized in air at 900 $^0$C were also measured in ref. [5]. From the known creep properties of the steel the values of the growth stresses in the $Cr_2O_3$ could be calculated. They ranged between -1600 and -300 MPa depending on the scale thickness. As the specimens were flat, these are intrinsic growth stresses and therefore caused by the lateral components of the oxidation strain tensor.

From the results of ref. [5] we could estimate the magnitude of the lateral components, but this would not help us for the situation of duplex scales. In view of the uncertainty on the magnitude of the lateral oxidation strain components we consider in the following only the most simple case that only the orthogonal component is non-vanishing. For this situation we can establish simple formulas for the growth stresses in duplex scales in the same way as has been done in ref. [6] for a single-layered oxide scale. The essential point is the nature of the oxidation process, namely at which location the new oxide is formed [7,8]. It is generally accepted that the magnetite subscale grows at the outer surface and the Fe/Cr spinel subscale at the interface with the metallic substrate.

### 2.2a   Geometrically-induced growth stresses

We assume that the oxidation strain tensor has the following form:

$$\overrightarrow{\varepsilon}^{sp/ma} = (\varepsilon_r^{sp/ma}, 0, 0) \tag{13}$$

with:

$$\varepsilon_r^{sp/ma} = \Phi^{sp/ma} - 1 \tag{14}$$

The following simple distribution for the geometrically-induced growth stresses in a duplex scale by using the principles of Manning [7] in the same way as has been done in ref. [6] for a single layer oxide scale growing at the interface with the metallic substrate can be derived:

$$\sigma_\Theta^{gr,sp}(t) = \frac{\varepsilon_r^{sp}}{\Phi^{sp}} \cdot \frac{\delta^{sp}}{a} \cdot E^{sp} \cdot t \tag{15}$$

$$\sigma_\Theta^{gr,ma}(t) = \frac{\varepsilon_r^{ma}}{\Phi^{ma}} \cdot \frac{\delta^{ma}}{a} \cdot E^{ma} \cdot (t-1) \tag{16}$$

$\Phi$ =    Pilling-Bedworth ratio
$t$ =    dimensionless distance from the inner radius of the subscale, $t = [0,1]$
$a$ =    $r^{cl}_{out}$ for a convex surface = $- r^{cl}_{in}$ for a concave surface

The difference between the magnetite and spinel sublayers arises from the location of oxide growth. Whereas magnetite grows outwards at the surface, the spinel sublayer grows inwards at the interface with the metallic substrate.
The mean hoop stresses in both subscales are then given as:

6

$$\overline{\sigma_{\Theta}^{gr,sp}} = 1/2 \cdot \frac{\varepsilon_r^{sp}}{\Phi^{sp}} \cdot \frac{\delta^{sp}}{a} \cdot E^{sp} \tag{17}$$

$$\overline{\sigma_{\Theta}^{gr,ma}} = -1/2 \cdot \frac{\varepsilon_r^{ma}}{\Phi^{ma}} \cdot \frac{\delta^{ma}}{a} \cdot E^{ma} \tag{18}$$

The axial growth stresses in both subscales are determined by the condition of plane strain ( $\varepsilon_z = 0$ ):

$$\overline{\sigma_z^{gr,sp/ma}} = -\nu_{sp/ma} \cdot \overline{\sigma_{\Theta}^{gr,sp/ma}} \tag{19}$$

It should be noted that Manning [7] has concluded that the geometrically-induced growth stresses in a duplex scale are zero by simply adding the displacement vectors of the subscales. But we think that each subscale must be treated separately and that his conclusion is therefore not correct.

**2.2b**                           **Intrinsic growth stresses**

If there are lateral components in the oxidation strain tensor, we would have intrinsic growth stresses, which would add to the geometrically-induced components. The magnitude of the intrinsic growth stresses can be estimated with the help of the following expression:

$$\sigma_{\Theta}^{\text{int } r.gr.} = \sigma_z^{\text{int } r.gr.} = \frac{-E^{sp/ma}}{1-\nu_{sp/ma}} \cdot \varepsilon_{lat.}^{sp/ma} \tag{20}$$

There we have assumed that the circumferential and axial components of the oxidation strain tensor are equal:

$$\varepsilon_{lat.}^{sp/ma} = \varepsilon_{\Theta}^{sp/ma} = \varepsilon_z^{sp/ma} \tag{21}$$

**2.2c    Growth stresses due to internal oxidation**

To the knowledge of the author of this report the effect of internal oxidation on the growth stresses has not yet been treated in the literature. We are attempting for the first time to deal with this problem with the help of simple methods.

The work of ref. [9] on the stresses caused by a spherical inclusion in a metal matrix due to temperature changes could be used to describe the growth stress distribution

7

in and around one oxide particle in a metal matrix. The growth stresses in the oxide particle are therefore given as:

$$\sigma_r^{o.p.} = \sigma_\vartheta^{o.p.} = \sigma_\varphi^{o.p.} = \sigma_{ox} = \frac{-\varepsilon_{ox}}{(1 + \nu_{me})/2 \cdot E_{me} + (1 - 2 \cdot \nu_{ox})/E_{ox}} \tag{22}$$

$r, \varphi, \vartheta$ = coordinates of the spherical system
$\varepsilon_{ox}$ = oxidation strain
In the metallic matrix we have the following stress distribution:

$$\sigma_r^{me} = \sigma_{ox} \cdot (\frac{R^{o.p.}}{r})^3 \tag{23}$$

$$\sigma_\vartheta^{me} = \sigma_\varphi^{me} = -1/2 \cdot \sigma_{ox} \cdot (\frac{R^{o.p.}}{r})^3 \tag{24}$$

$R^{o.p.}$ = radius of the oxide particle
The problem is that we have a many-particle problem. That means we have to consider the superposition of stresses caused by the presence of many particles. For the time being we don't have the general solution for this problem.

But the topological conditions might be even more complicated, also we do not know whether the oxide particles are really of a spherical shape. Therefore we treat the problem in a completely different, simpler way. We consider the zone of internal oxidation as a mixture of metal and oxide, whose mechanical properties may be calculated with the help of simple mixture rules. Let the volume fraction of the oxide be $f_{ox}$ then the metal fraction $f_{me}$ is $1 - f_{ox}$ and the Young's modulus in the internal oxidation zone and the respective Poisson ratio are given as:

$$E^{i.o.z.} = f_{ox} \cdot E_{ox} + f_{me} \cdot E_{me} \tag{25}$$

$$\nu^{i.o.z.} = f_{ox} \cdot \nu_{ox} + f_{me} \cdot \nu_{me} \tag{26}$$

If the oxide has the shape of small spherical particles the oxidation strain in the internal oxidation zone should be isotropic and should therefore be given by the following expression:

$$\varepsilon_{ox}^{i.o.z.} = f_{ox} \cdot (\Phi^{1/3} - 1) \tag{27}$$

8

$\overset{\triangleright}{\Phi}$ = modified Pilling-Bedworth ratio (modification due to vacancy annihilation)

The stress state due to this isotropic oxidation strain is, of course, compressive and bi-axial:

$$\sigma_\Theta^{i.o.z.} = \sigma_z^{i.o.z.} = \frac{-E^{i.o.z.}}{1 - \nu^{i.o.z.}} \cdot \varepsilon^{i.o.z.} \tag{28}$$

The expressions in eq. (28) are viewed to be volume averaged stresses in the internal oxidation zone. The upper limit should be given by the yield stress in the metallic matrix.
For the time being we have no indications for mechanical problems in the internal oxidation zone. Also, we have no experimental values for the parameters of the model as for $f_{ox}$ and $\overset{\triangleright}{\Phi}$. Therefore we do not continue with this model.

As a general remark for all the oxidation processes it should be noted that upon oxidation an annihilation of vacancies could occur, if there are any in the metal matrix. This mechanism has been discussed in [7] and [10], it would lead to reduced growth stresses. As we have for the time being no idea about the amount of vacancies in the steels of interest, we have neglected this effect. In the internal oxidation zone we would expect vacancies, as Fe and other metal atoms are migrating to the oxide scale.

## 2.3 Superposition of growth and thermal stresses

The formulas for the growth stresses and that for thermal cycling were derived under the premises that the strains in the oxide scale and the metallic substrate are purely elastic (no plastic strain formation, no cracking effects). Thus, we can linearly superpose in both subscales the growth stresses and the stresses due to a temperature change in order to obtain the total stress at a certain temperature T during the ramp:

$$\overline{\sigma_{\Theta,z}^{sp/ma}}(T) = \overline{\sigma_{\Theta,z}^{gr,sp/ma}} + \Delta\sigma_{\Theta,z}^{therm,sp/ma}(T) \tag{29}$$

## 2.4    Elastic strain energy in the oxide scale

We have now available all the elements for the calculation of the elastic strain energy in both subscales, parameters which we need in criteria for cracking and spalling:

$$W_{el}^{sp} = 1/2 \cdot (\overline{\sigma_{\Theta}^{sp}} \cdot \overline{\varepsilon_{\Theta}^{el,sp}} + \overline{\sigma_z^{sp}} \cdot \overline{\varepsilon_z^{el,sp}}) \cdot \delta_{sp} =$$
$$\frac{\delta_{sp}}{2 \cdot E_{sp}} \cdot (\overline{\sigma_{\Theta}^{sp}} \cdot (\overline{\sigma_{\Theta}^{sp}} - v_{sp} \cdot \overline{\sigma_z^{sp}}) + \overline{\sigma_z^{sp}} \cdot (\overline{\sigma_z^{sp}} - v_{sp} \cdot \overline{\sigma_{\Theta}^{sp}})) \qquad (30)$$

$$W_{el}^{ma} = 1/2 \cdot (\overline{\sigma_{\Theta}^{ma}} \cdot \overline{\varepsilon_{\Theta}^{el,ma}} + \overline{\sigma_z^{ma}} \cdot \overline{\varepsilon_z^{el,ma}}) \cdot \delta_{ma} =$$
$$\frac{\delta_{ma}}{2 \cdot E_{ma}} \cdot (\overline{\sigma_{\Theta}^{ma}} \cdot (\overline{\sigma_{\Theta}^{ma}} - v_{ma} \cdot \overline{\sigma_z^{ma}}) + \overline{\sigma_z^{ma}} \cdot (\overline{\sigma_z^{ma}} - v_{ma} \cdot \overline{\sigma_{\Theta}^{ma}})) \qquad (31)$$

## 2.5    Cracking and spalling of oxide scales

The failure mechanisms in oxide scales under tensile or compressive stresses have been discussed by Evans in a review paper [10]. It was concluded that tensile stresses within the oxide layer can readily produce through-scale cracking but that spalling of the oxide is difficult. For compressive stresses there are two routes for spalling. Route I , a wedging mechanism, should occur for strong interfaces and weak oxide scales, and route II , a buckling mechanism, for weak interfaces and strong oxide scales.
Elasticity theory [11] gives the following expression for the critical buckling stress:

$$\sigma_b = \frac{1.22 \cdot E_{ox}}{1 - v_{ox}^2} \cdot (\frac{\delta_{ox}}{R})^2 \qquad (32)$$

R = radius for area of decohesion
As the stresses in the oxide scale comprise at most only a few per cent of $E_{ox}$, a buckling mechanism is only expected for R much larger than $\delta_{ox}$ , that means for thin oxide scales with large pores or other large flaws at the interface.
The wedging mechanism (route I) can be treated with the elastic strain energy criterion described below [10].

Protective oxide layers display brittle characteristics at temperatures below the brittle-to-ductile transition temperature. Hence, in the temperature range of interest for accelerator driven systems one can apply the theory of Griffith. This theory stipulates that a flaw in the scale will continue to grow under a stress $\sigma_f$ in the oxide scale if its strain energy release G exceeds the critical energy release rate $G_c$ of the oxide:

$$G \geq G_c \qquad (33)$$

where

$$G = K^2/E \tag{34}$$

and the stress intensity factor K:

$$K = F \cdot \sigma_{ox} \cdot (\Pi \cdot c)^{1/2} \tag{35}$$

c = flaw size

F is a numerical factor, which depends on the shape and position of the flaw. F has a, for example, a value of 1.12 for a surface notch of depth c and infinite length.
The critical energy release rate $G_c$ is related to the surface energy $\gamma_s$ :

$$G_c = \gamma_s \tag{36}$$

$\gamma_s$ = surface energy

Hence, we obtain the following criteria for fracture:

$$\frac{\sigma_{ox}^2 \cdot F^2 \cdot \Pi \cdot c}{Eox} \geq \gamma_s \tag{37}$$

The flaw size c is normally not very well known, but one can assume that it increases with the scale thickness [12]:

$$c = f \cdot \delta_{ox} \tag{38}$$

In ref. [12] a value of 0.2 is proposed for f. With this value we obtain the following criteria:

$$\frac{\sigma_{ox}^2}{E_{ox}} \cdot \delta_{ox} \cdot 0.785 \geq \gamma_s \tag{39}$$

For a bi-axial stress state in the oxide scale we obtain the following expression for the total elastic strain energy in the scale:

$$G_{el} = \frac{\sigma_{ox}^2}{E_{ox}} \cdot (1. - \nu_{ox}) \cdot \delta_{ox} \tag{40}$$

This expression is similar to that in the left hand side of () and in view of the uncertainties on the shape and position of the flaws we may use the following global criteria for spalling:

$$G_{el} \geq \gamma_s \tag{41}$$

The physical meaning of the criteria () implies that spalling occurs when the whole elastic strain energy is sufficient for the formation of new surfaces.

The parameter $\gamma_s$ can take different values depending on the location of spalling, especially for duplex scales. Spalling can occur at the interface with the metallic substrate or at the interface between the two subscales or within one of the two subscales. The value of the surface energy $\gamma_s$ may, for example, be lowered by the presence of pores or other cavities.

As far as is known to the author of this note, the failure criterion (41) has only been applied to pure bi-axial compressive stress states. Whether it is also sufficient for a mixed stress state (tensile and compressive stress components) is an open question.

A different approach for the treatment of cracking in multi-layered materials has been adopted in refs. [27] and [28]. Based on elastic stress solutions at the crack tip the following expression for the energy release rate was derived in case of a bi-axial tensile stress state:

$$G_{el} = (1 + \nu_{ox}) \cdot Z \cdot W_{el} \tag{42}$$

The non-dimensional parameter Z takes on different values depending on the failure mode. A list of values for Z is given in ref. [27]. For debonding the value at initiation is 1.028 and at steady-state it is 0.5. The failure criterion of eq. (41) was also adopted. Thus, this approach would lead to somewhat different results depending on the failure mode.

It should be noted that eq. (41) gives the lower bound for cracking but that the incidence of cracking or decohesion is probabilistic in nature depending on the cavities in the oxide scale.

## 3.    Material data

In Fig. 1 are plotted different thermal expansion coefficients versus the temperature T (in $^0$C) for materials which are of interest to us for the treatment of duplex scales on stainless steels. The data on austenitic and ferritic steels are from Petersen [13], the data for magnetite from Armit et al [12], and the data on Fe/Cr spinel and on the martensitic steel P92 from Osgerby [14]. For the time being we assume that it is representative for other martensitic steels as well. But this can only be checked, when further data on thermal expansion coefficients could be found in the literature. It should also be noted that in ref. [12] the thermal expansion coefficient of AISI 316 is given and that this curve is very near to that from ref. [13] for austenitic steels.

Data on Fe/Cr spinel could only be found in ref. [14], the respective curve is similar to that for magnetite. It could be expected that the thermal expansion coefficient of the

Fe/Cr spinel depends on the Cr content. In ref. [14] the Cr content of the spinel is not noted, also no reference on the data was given.

In ref. [14] the data are considered as mean values of the thermal expansion coefficients (see figure 8 of ref. [14]) and the results of stress calculations indicate that the data were used in such a way. But the data given in ref. [14] were partially taken from ref. [12] (for example that for magnetite and that for haematite) and the authors in ref. [12] were fully aware that the thermal strain must be calculated by summing over small temperature intervals (see page 4-2 of ref. [12]. There is also the good agreement of the curves for austenitic steels from ref. [13] with that for AISI 316 from ref. [12]. Therefore we think that in ref. [14] an improper use of the data on thermal expansion coefficients has been made leading to erroneous stress values.

Table 1 Summary of mechanical properties used for the calculations

|  | $Fe_3O_4$ | $FeCr_2O_4$ |
|---|---|---|
| Young's modulus $E_{ox}$ in MPa | $2.1\ 10^5$ | $2.33\ 10^5$ |
| Poisson ratio $\upsilon$ | 0.29 | 0.31 |
| Surface fracture energy $\gamma_s$ in J/m$^2$ | 4.5 | 5.0 |
| Fracture toughness $K_{Ic}$ in MPa*m$^{1/2}$ | 1.4 | 1.5 |
| $\gamma_s$*$E_{ox}$ in MPa$^2$*mm | 945. | 1165. |
| Pilling-Bedworth ratio $\Phi$ | 2.07 | 2.07 |

In Table 1 we have listed the mechanical properties for the two oxide phases, which have been used for the calculations. They were taken from ref. [15] and [16]. These properties are generally dependent on the temperature. But as the Young's moduli of the oxides, for example, are often only known for room temperature [16], we have to use them as average values valid for the whole temperature range. The fracture toughness values of many oxides, on the other hand, are known to be fairly constant between 0 and 600 $^0$C [16].

There are also experimental data on oxide scale failure strains to be found in the literature. For example, in ref. [15] data for 9 at% Cr steel and for AISI 316 can be found and in ref. [17] data for oxide scales on mild steel. The failure strains depend on many parameters, the most important ones seem to be the temperature, the strain rate, the mode of loading and above all the oxide scale thickness. We have transformed the failure strains $\varepsilon_f$ into values of the failure stress $\sigma_f$ assuming a bi-axial stress state:

$$\sigma_f = \frac{E_{ox}}{1 - \nu_{ox}} \cdot \varepsilon_f \qquad (43)$$

In Fig. 2 we have only plotted the lower bounds of the failure stress for the data of [15] and [17]. We can note that there is a clear tendency for the failure stress to decrease with increasing oxide scale thickness.
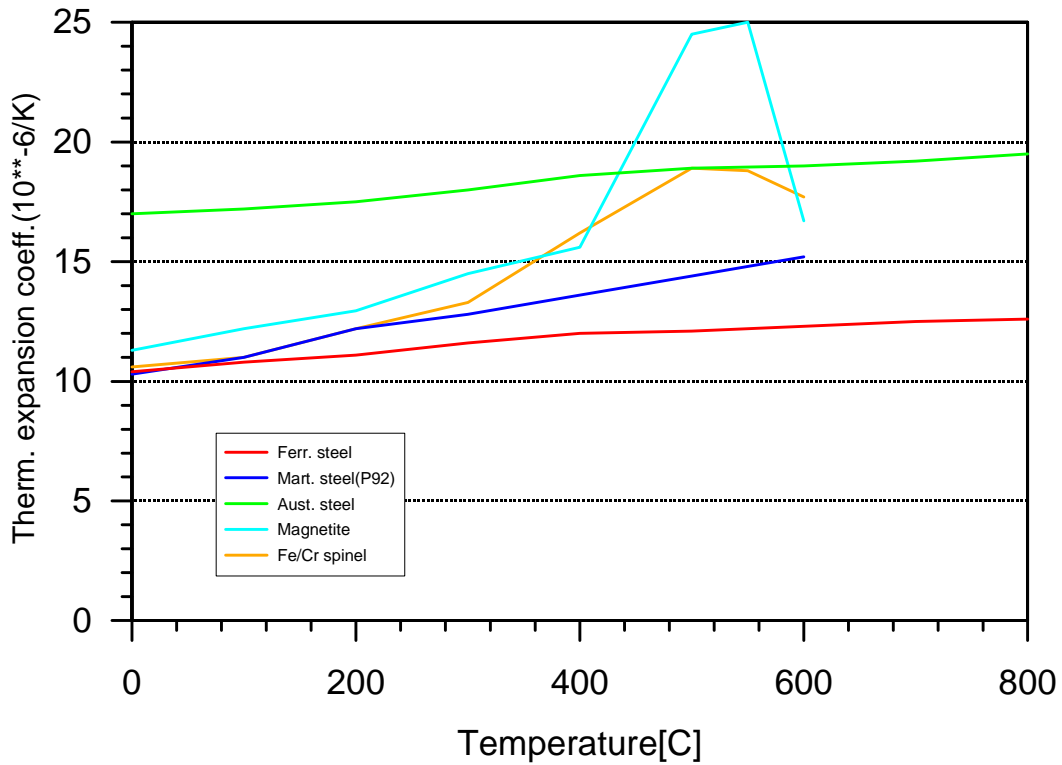
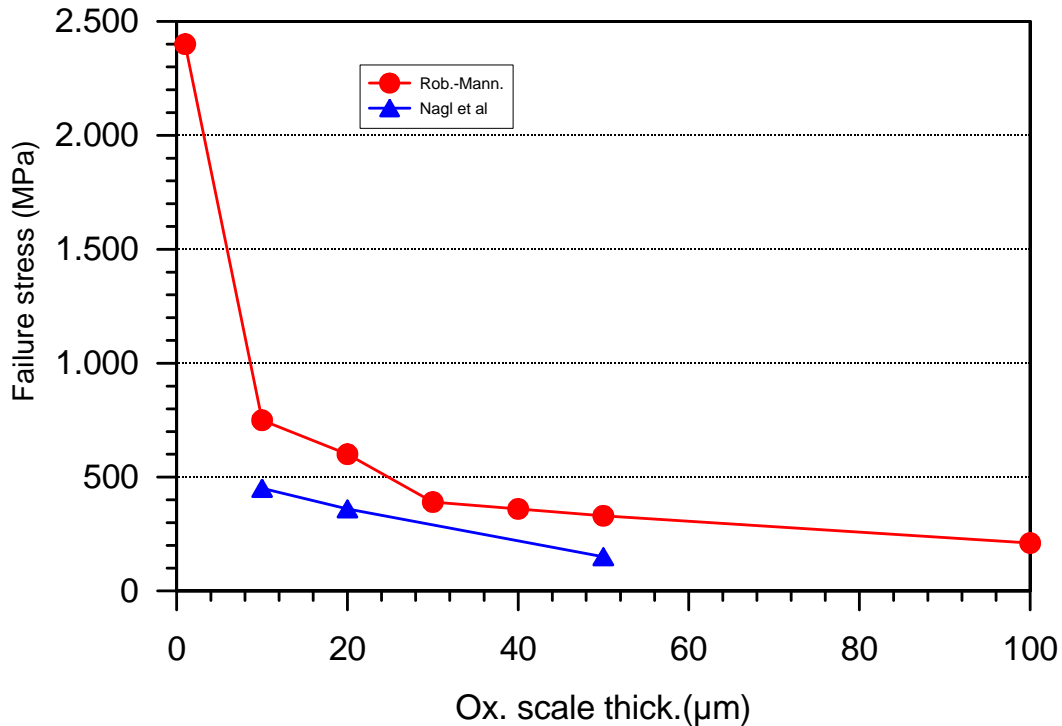Fig.1 Thermal expansion coefficients of different stainless steels and iron oxides



Fig. 2 Failure stress of iron oxide scales (lower bound) versus oxide scale thickness

## 4.    Results of stress calculations

In the following we are going to discuss the results of stress calculations starting with the stresses due to temperature changes.

In Fig. 3 are plotted the thermal hoop stresses as a function of the temperature change into the ramp for the three types of steels, which are of interest to us (martensitic, ferritic and austenitic steels), under isothermal conditions in the magnetite and Fe/Cr spinel subscales. For austenitic steels the hoop stresses are mainly compressive with the mechanical load in the spinel subscale being higher in absolute magnitude by about 30%. The stresses in case of martensitic and ferritic steels are tensile in both subscales. The highest tensile stresses are to be found in the magnetite subscale on ferritic steels and the lowest stresses in the Fe/Cr spinel on martensitic steels. Thus, martensitic steels compare favourably to austenitic and ferritic steels under thermal cycling.

In case of non-isothermal conditions the thermal stresses in the oxide scales on austenitic steels would be less compressive and for ferritic and martensitic steels more tensile, as the drop of the mean temperature in the metallic substrate is generally smaller than the drop in the oxide scales on test specimens.

Evans et al [10] have given the mechanical strains due to a temperature drop for different oxides on metallic substrates. In most cases the strain in the oxide scale increases strictly linearly with the temperature drop. This is a consequence of the assumption of temperature independent thermal expansion coefficients taken by these authors. For a $FeCr_2O_4$ scale on a Fe18Cr8Ni steel the mechanical strain amounts to about -0.7 % for a temperature drop of 600 $^0C$ corresponding to a compressive stress of about 1631 MPa. For a magnetite scale on a Fe9Cr1Mo steel a strain of -0.2 % is given for the same temperature drop corresponding to a tensile stress of about 420 MPa. It should be noted that in ref. [10] not the normal sign convention for stresses is used but a reversed one.

The thermal stresses shown in ref. [14], increase in magnitude only for the first 150 $^0C$ of the temperature ramp. This is evidently a consequence of the peak in the thermal expansion coefficients in the magnetite and spinel oxide phases. But for higher temperature ramps the thermal stresses decrease and are practically zero at 0 $^0C$ that means after a temperature ramp of 600 $^0C$. This is a very strange behaviour and contradicts all that is known from the literature. We think that this is due to a misunderstanding on the importance of the thermal expansion coefficients. The temperature dependent values have presumably been used as mean thermal expansion coefficients, and as the values at 0 $^0C$ of the oxides and of the steel are near together the calculated thermal stresses of ref. [14] are very small. It should be noted that the thermal stresses given in [14] are relatively small for all the subscales over the whole temperature range and in the maximum less than 100 MPa.

In Fig. 4 we have plotted the mean growth stresses in both subscales as a function of the subscale thickness for two values of the outside radius of the metallic cylinder. In the magnetite subscale we have compressive growth stresses, as the oxidation occurs at the outside of this subscale, and in the Fe/Cr subscale we have tensile growth stresses, as the oxidation occurs at the inside of the subscale. The growth stresses increase linearly with the subscale thickness and decrease linearly with increasing radius of curvature. For a flat surface the geometrically-induced growth stresses would be zero, as the radius of curvature is infinite. For thin wires, on the other hand, geometrically-induced growth stresses can become a severe problem. For concave surfaces the signs of the growth stresses would be reversed.

We are now going to consider the combined effect of growth and thermal stresses for our standard case. The thickness of the subscales is taken as a parameter, that means the specimens are oxidized up to a certain value for the thickness of the duplex scale at a certain oxidation temperature and then a downwards temperature ramp is applied. In reality, the thickness values of both subscales are slightly different, but for the sake of simplicity we assume in the following that both subscales have equal thickness. For the oxidation temperature we have taken a value of 550 $^0$C.

In Fig. 5-7 we have plotted for martensitic steels the mean hoop and axial stresses in both subscales versus the temperature during the ramp starting with the oxidation temperature of 550 $^0$C. The highest stresses are the axial component in the magnetite subscale and the circumferential component in the Fe/Cr spinel, which are near together in magnitude. These components increase with the subscale thickness. The other two components decrease with increasing subscale becoming compressive for an ever greater temperature range.

It is obvious that we have now a relatively complex stress state in both subscales and not simply a bi-axial one, the axial and the circumferential component being very different in magnitude and depending on the subscale thickness and the temperature. Under such circumstances it is very difficult to assess the propensity for cracking or spalling of the subscales. One parameter which is certainly of relevance in this respect is the elastic strain energy in both subscales and eventually the sum of both. The results for these parameters are plotted in Fig. 8-10 together with the surface fracture energies of the Fe/Cr spinel and of magnetite.

It could be that there is tensile cracking caused by the tensile stress component. The plane of the tensile cracks would be orthogonal to this component. This would then mean that it no longer contributes to the elastic strain energy. But the other stress component would also be changed, as the premises for the stress calculation, that the material is a continuum, is no longer fulfilled. The formation of tensile cracks will perturb the in-plane stress distribution and also generate shear stresses [19]

The situation is much clearer for oxide scales on austenitic steels, as can be taken from Fig.11- 13. For low temperature differences all the stress components are in a compressive state. The temperature, where the stress changes from tensile to compressive is a bit different for the four components in the subscales and decreases with increasing subscale thickness for the hoop stress in the Fe/Cr spinel and the axial component in the magnetite subscale. The other two stress components are for all cases in a compressive state.

The tubing of the test loop CORRIDA is made of austenitic steel. For the tubing we encounter the situation of oxide scale formation on inner (concave) surfaces. For this reason we have done calculations for a radius of curvature of -4 mm.

In Fig. 14-16 the stress situation for such a case is exemplified. By comparison with Fig. 11-13 the influence of the radius of curvature can be deduced. . The hoop stress in the Fe/Cr spinel subscale is now deep in the compressive region also the axial component in the magnetite subscale.

In Fig.17 and 18 we have plotted for austenitic steels the hoop stress and the axial stress versus the subscale thickness with the temperature difference as a parameter ($\Delta T$ = -100K, -200 K, -300 K). Both stress components in the subscales increase

16

linearly in magnitude with the subscale thickness and are shifted downwards with higher temperature changes.

The combined effect of thermal and growth stresses has not very often been investigated in the literature. For alumina, scales, for example, the growth stresses at steady-state have been determined from measured residual stresses and from calculated values of thermal stresses (see for example ref. [23]). But for oxide scales on steels we do not know of such efforts. Often the investigation of stresses was for flat surfaces (see for example [18] and [19]) and in such cases there are no geometrically-induced growth stresses, and if one can neglect the intrinsic growth stresses the analysis would be correct.

We have plotted in Fig. 19-21 the elastic strain energy in both subscales and also the sum of both for three values of the subscale thickness for oxide scales on a convex surface on austenitic steels and compared this to the fracture surface energy of the Fe/Cr spinel and magnetite. For a subscale thickness of 10 µm the risk of spalling or scale detachment appears only for temperature changes of more than 300 K. In this regard an observation made in ref. [15] may be of great importance. It was found that for 9% Cr steels and for AISI 316 type steels only the magnetite sublayer spalled and the Fe/Cr spinel remained attached. These observations were for gas atmospheres, but we think that they might also be relevant for heavy liquid metal environments. This would then mean that only the release of the elastic strain energy in the magnetite subscale is relevant and not the sum for both subscales. In this case there is only a slight risk for magnetite spalling for temperature changes of about 500 K.

For subscale thickness values up to about 20 µm the risk for oxide scale spalling already at steady-state conditions seems small, whereas it seems high for subscales of 30 µm and more. According to our calculations we would expect that with oxide scales above about 40 µm mechanical effects should start to occur at steady-state. Furthermore, it seems rather improbable that values of 60 µm can be reached without severe damage.

It should be noted that our model is purely elastic, that means we have excluded any stress relief mechanisms like plastic flow or micro-cracking. For the calculation of the growth stresses we have not taken into account any annihilation of vacancies, an effect which would reduce the growth stresses. Also, there is a considerable uncertainty on the mechanical data for the iron oxides. The release of elastic strain energy can not only be achieved by spalling or detachment of the oxide scale but also by tensile or shear crack formation. Thus, the condition that the elastic strain energy must be above the surface fracture energy is a necessary condition but not in any case a sufficient one.
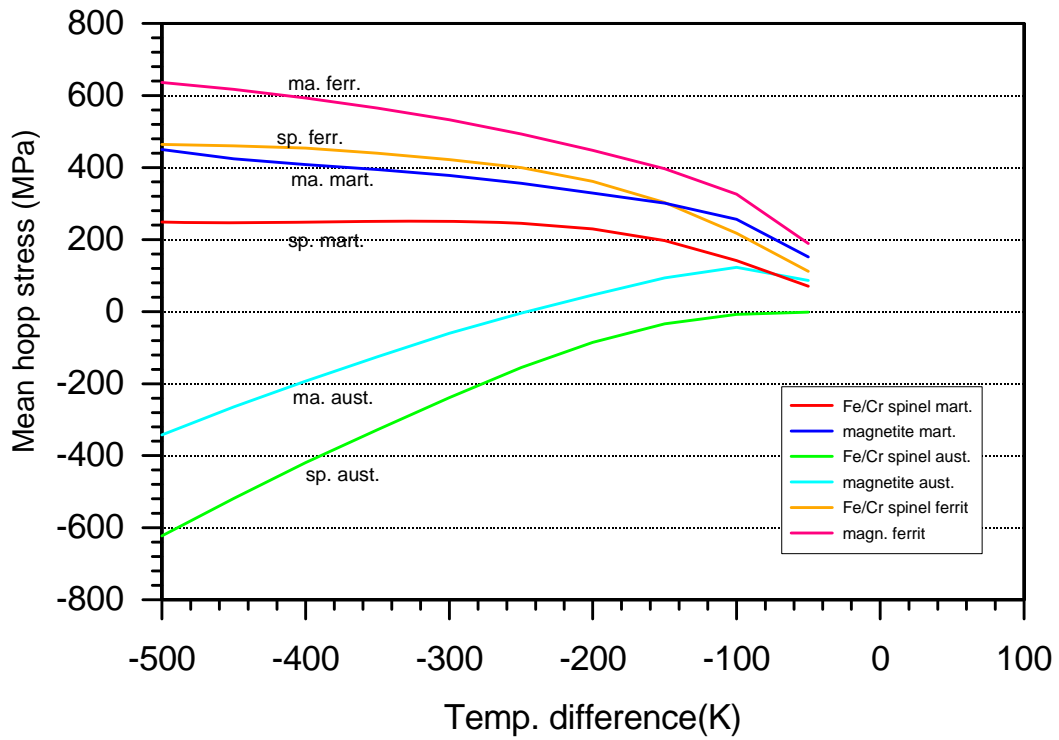
Fig. 3 Thermal stresses due to a downward temperature change for duplex scales on different stainless steels
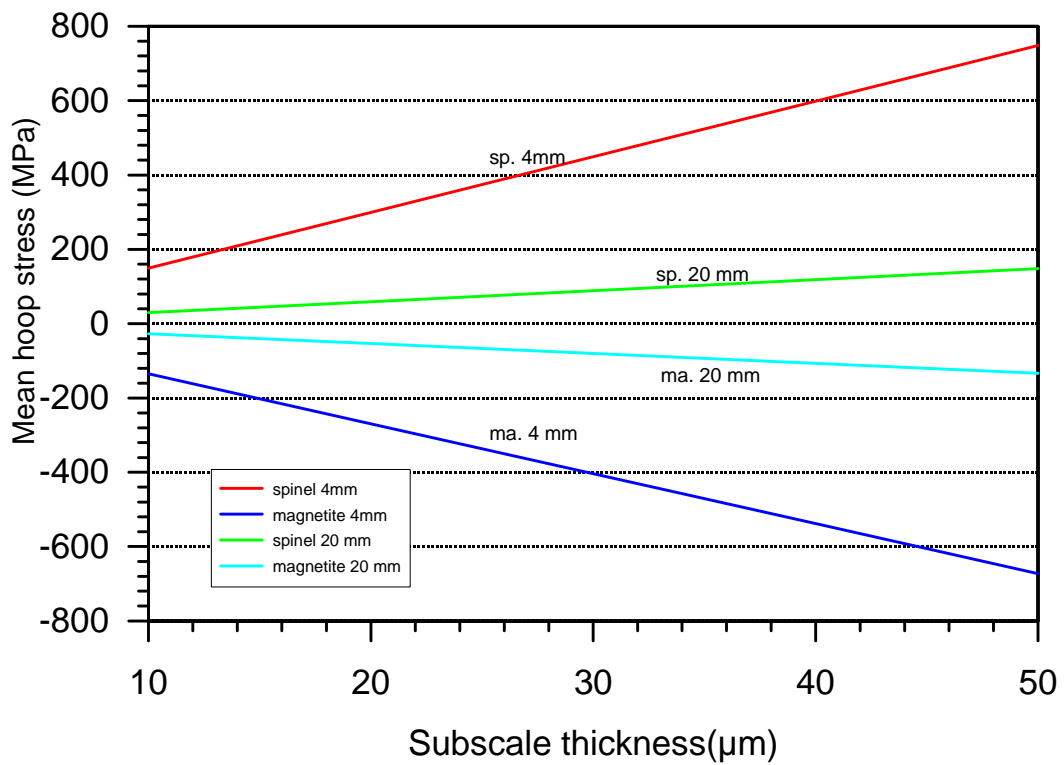


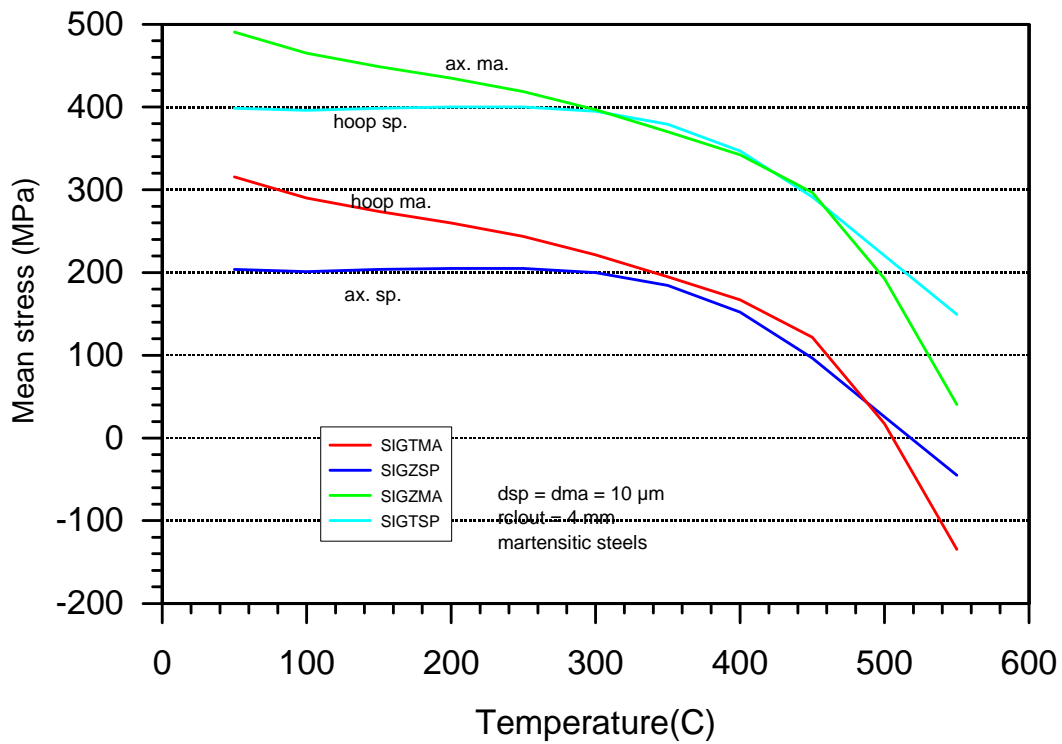Fig. 4 Geometrically-induced growth stresses in duplex scales

18

Fig. 5 Combined effect of growth and thermal stresses in the duplex scale on martensitic steels (subscale thickness 10 µm)
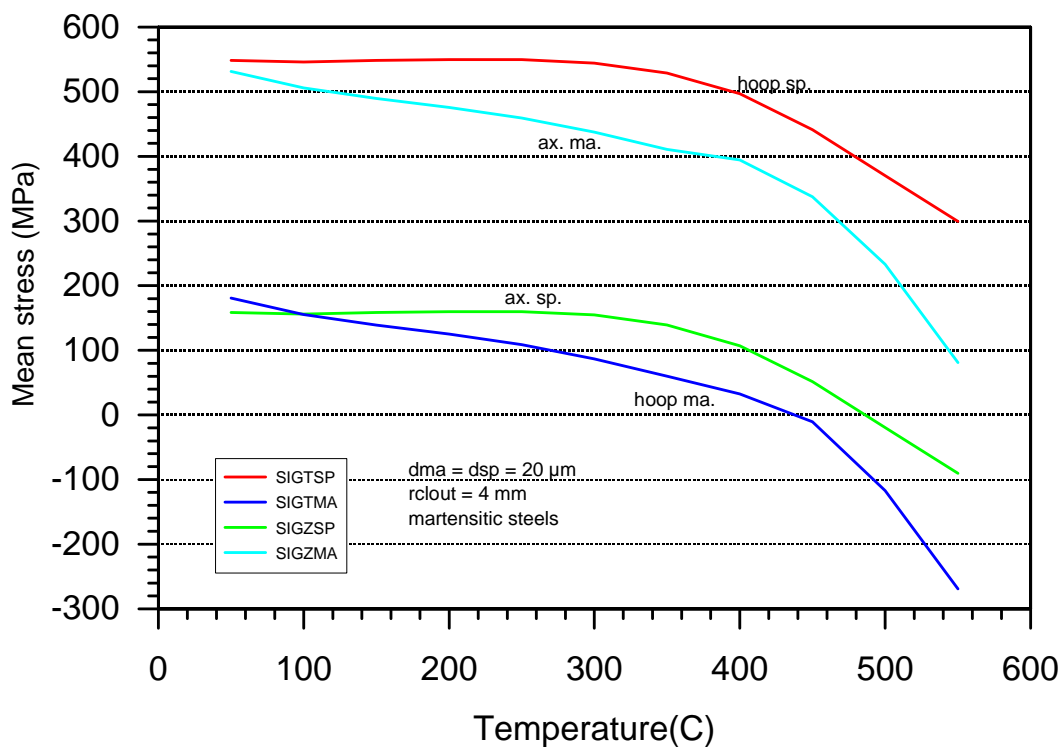


Fig. 6 Combined effect of growth and thermal stresses in the duplex scale on martensitic steels (subscale thickness 20 µm)
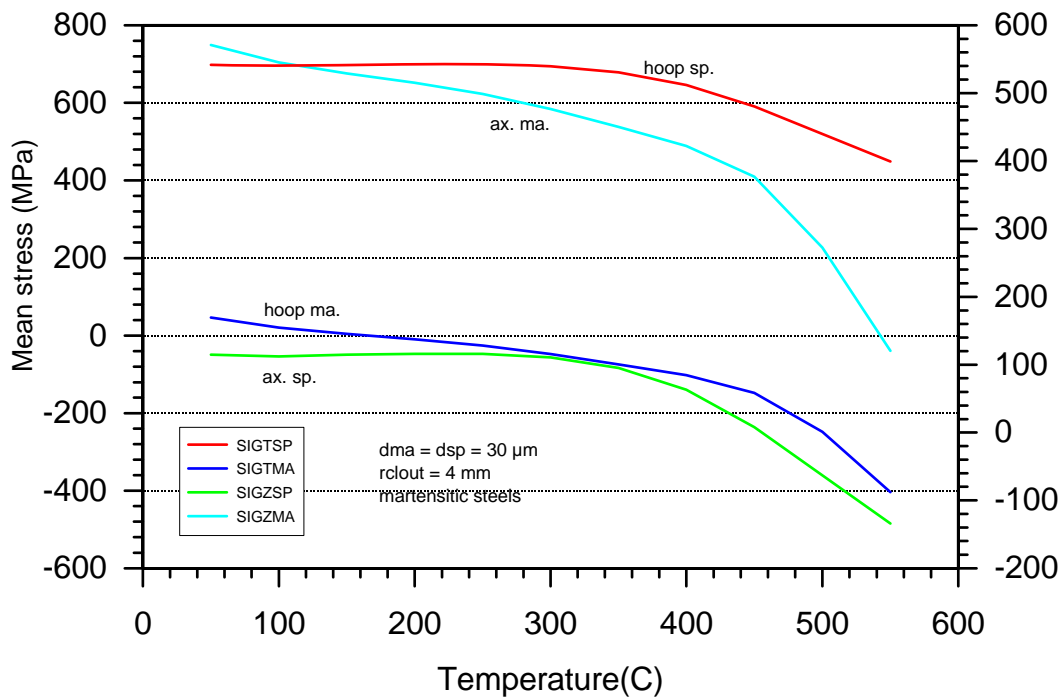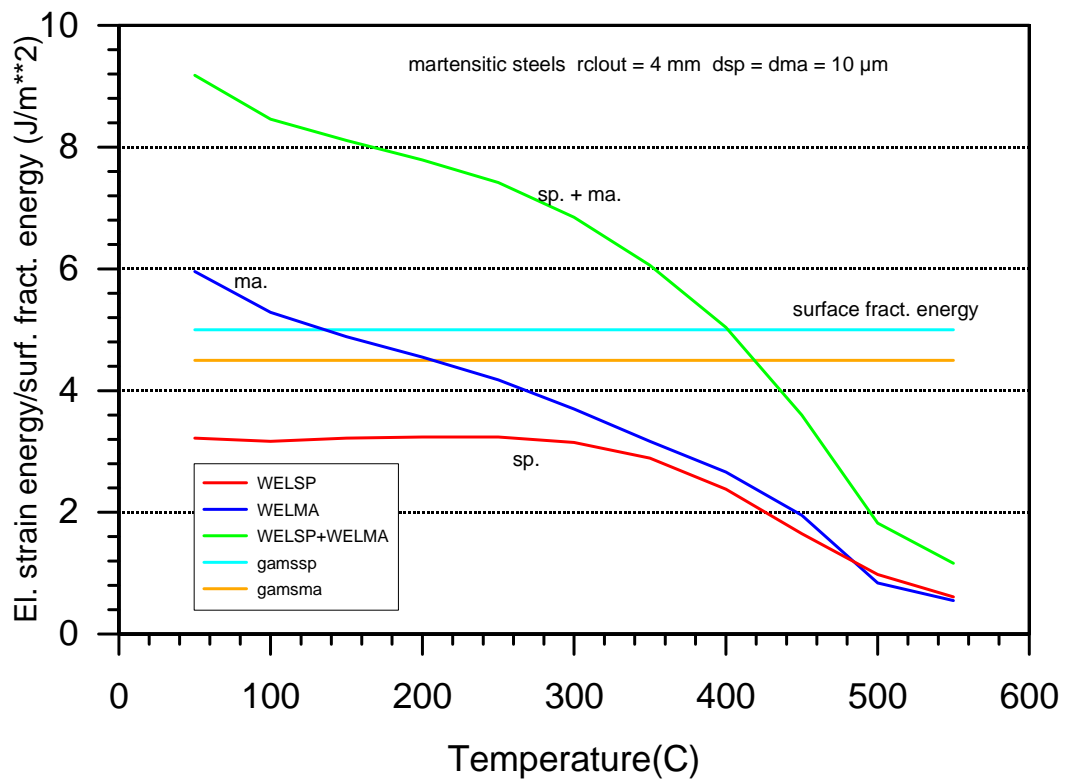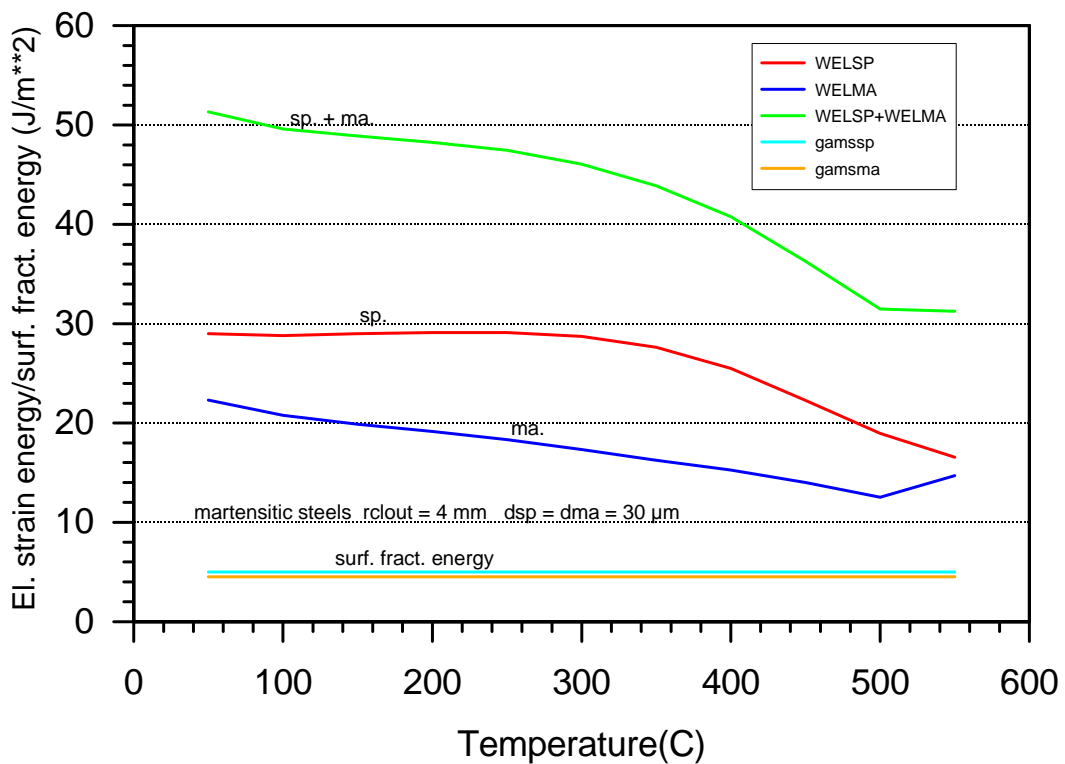
Fig. 7 Combined effect of growth and thermal stresses in the duplex scale on martensitic steels (subscale thickness 30 μm)

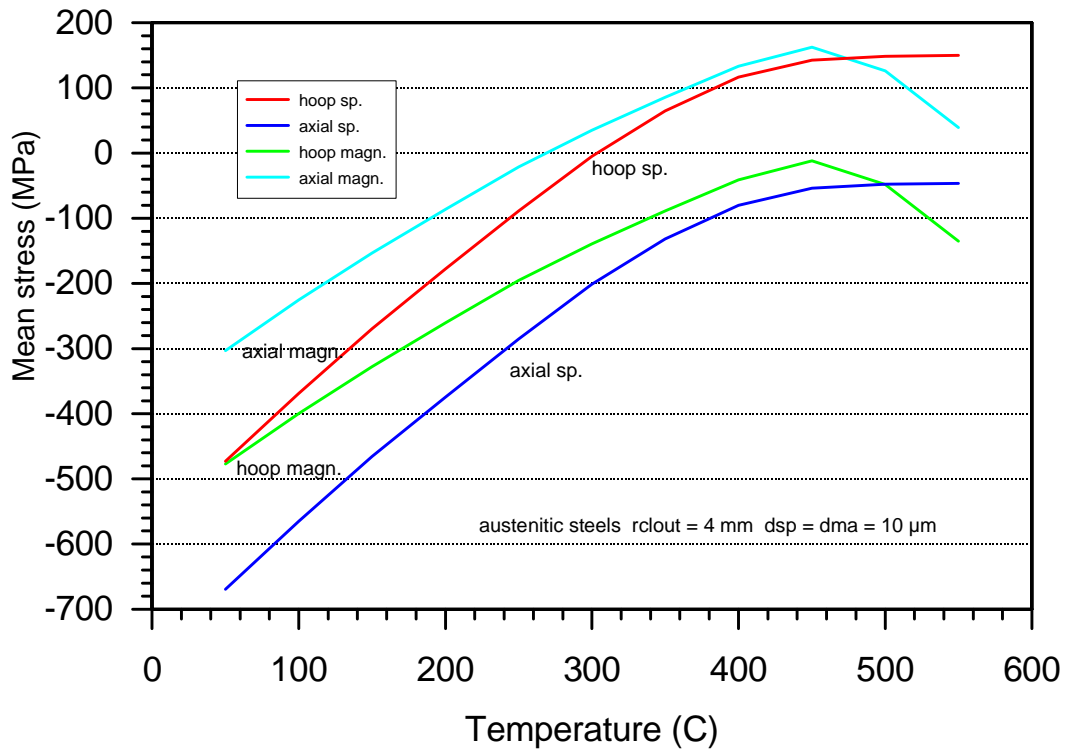Fig. 8 Elastic strain energy in the duplex scale on martensitic steels (subscale thickness 10 μm)
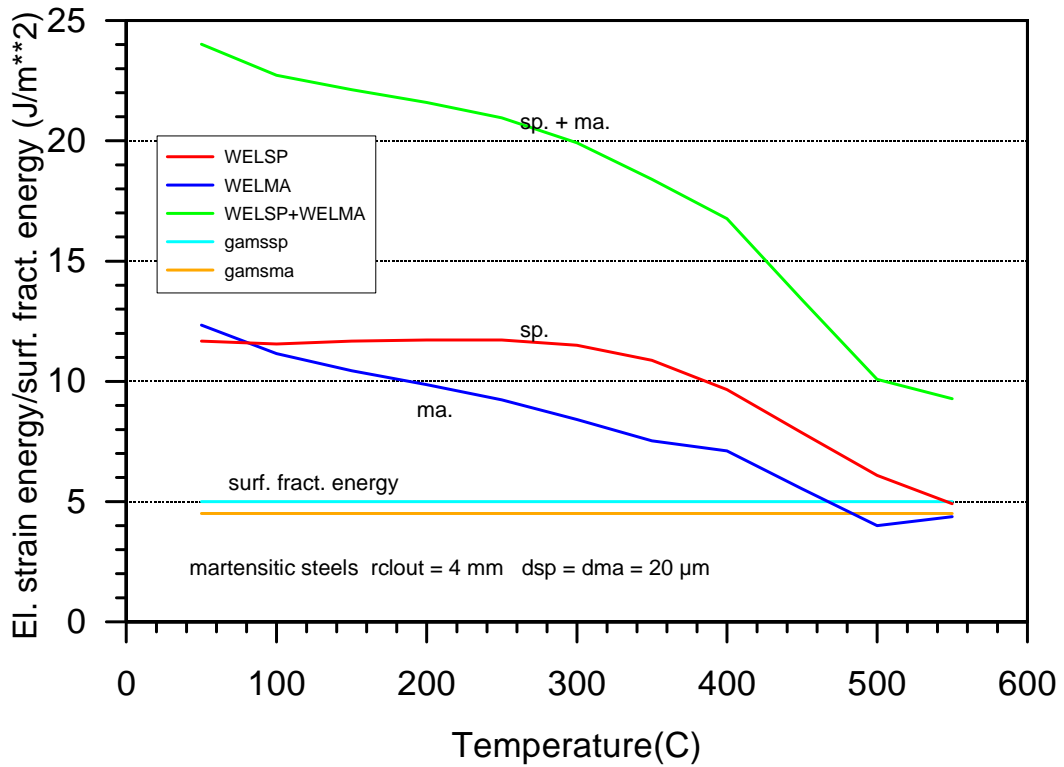
Fig. 9 Elastic strain energy in the duplex scale on martensitic steels (subscale thickness 20 μm)



Fig. 10 Elastic strain energy in the duplex scale on martensitic steels (subscale thickness 30 μm)

Fig. 11 Combined effect of growth and thermal stresses in the duplex scale on austenitic steels (convex surface, subscale thickness 10 μm)
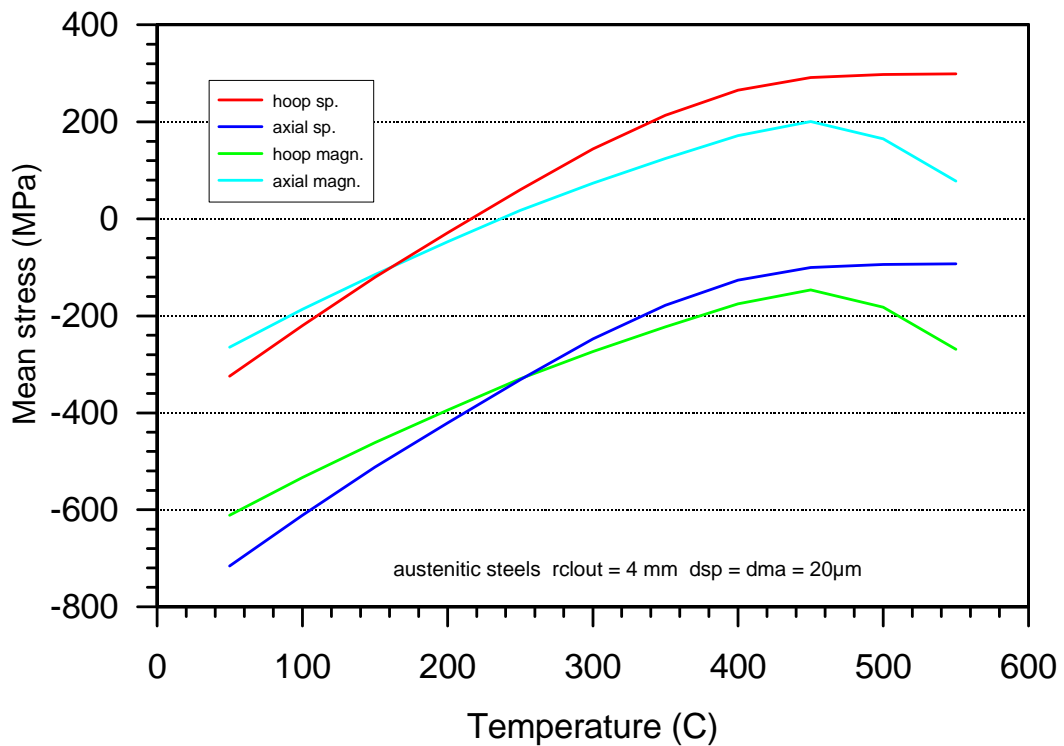


Fig. 12 Combined effect of growth and thermal stresses in the duplex scale on austenitic steels (convex surface, subscale thickness 20 μm)
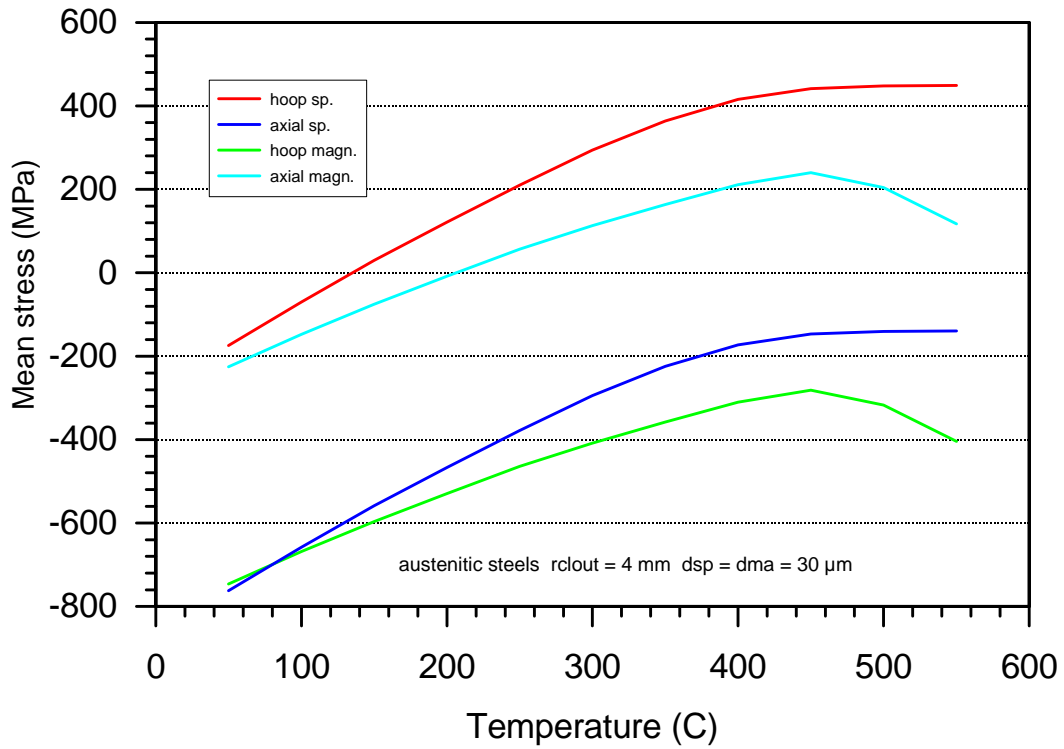
Fig. 13 Combined effect of growth and thermal stresses in the duplex scale on austenitic steels (convex surface, subscale thickness 30 μm)
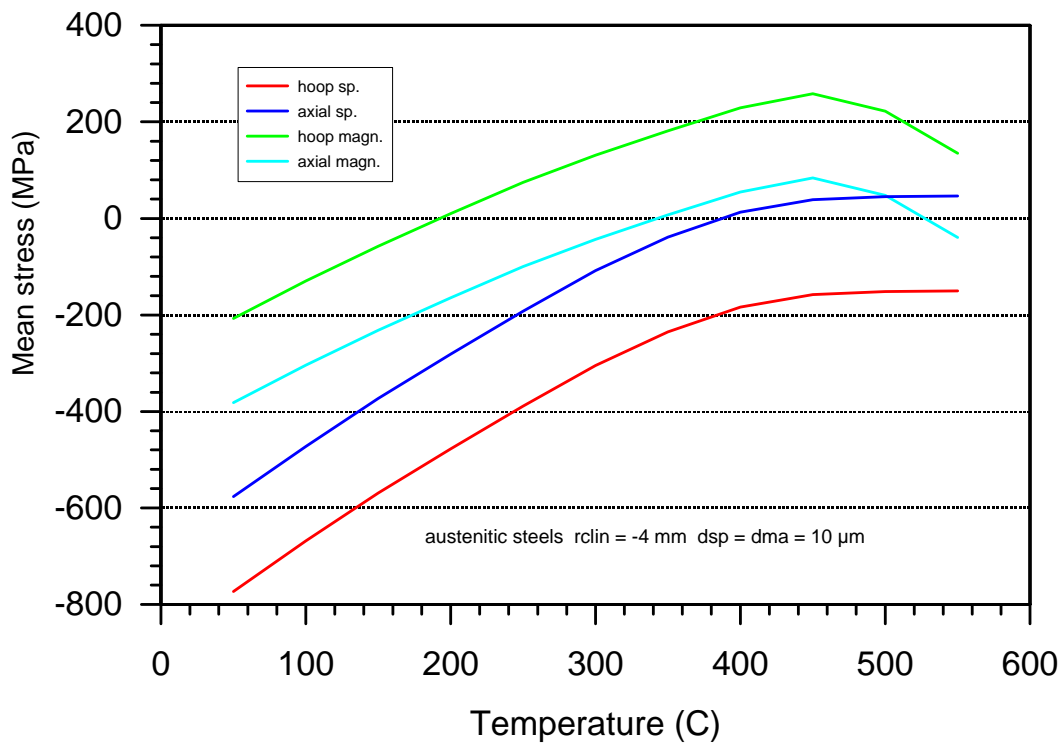


Fig. 14 Combined effect of growth and thermal stresses in the duplex scale on austenitic steels (concave surface, subscale thickness 10 μm)
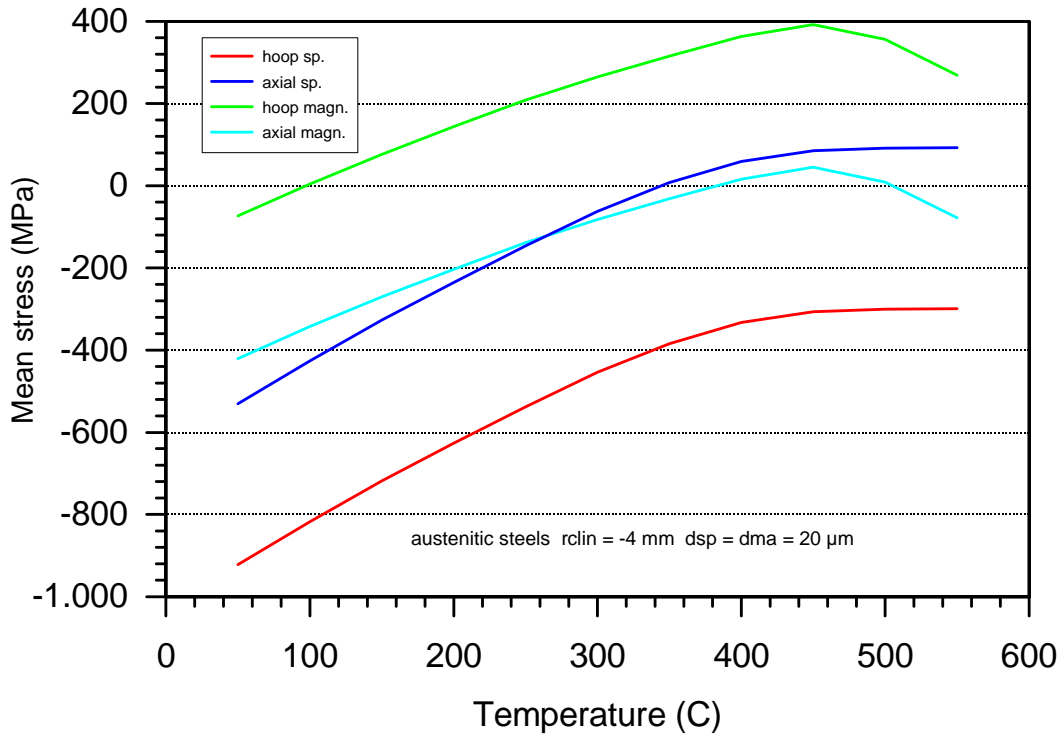
Fig. 15 Combined effect of growth and thermal stresses in the duplex scale on austenitic steels (concave surface, subscale thickness 20 μm)
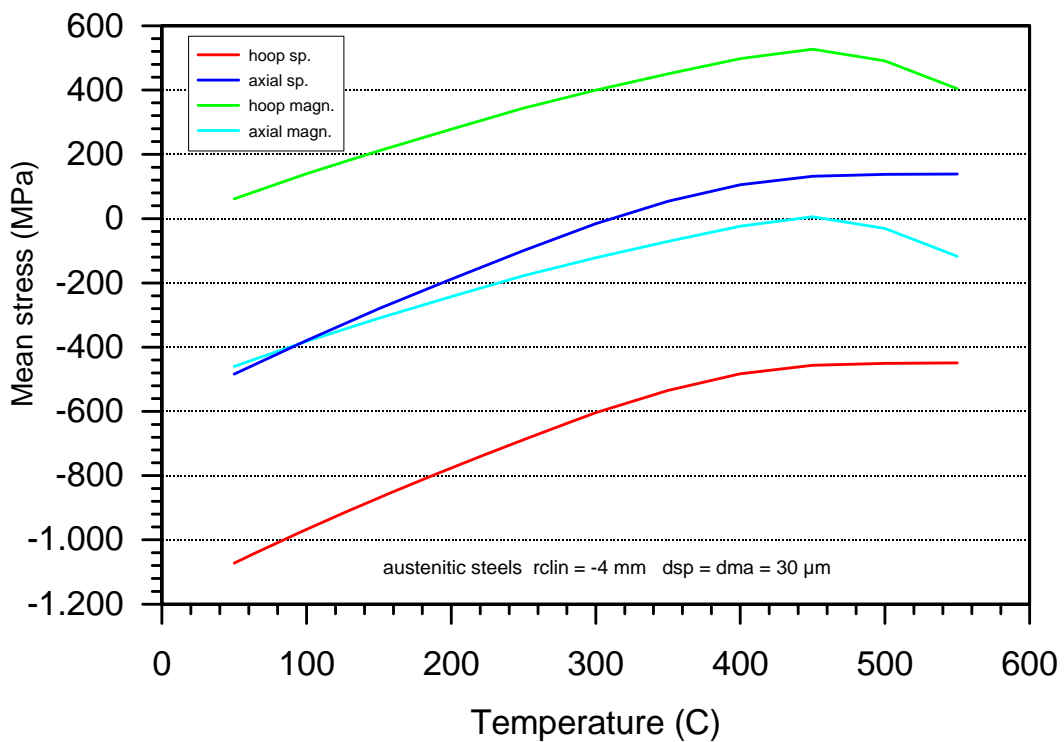


Fig. 16 Combined effect of growth and thermal stresses in the duplex scale on austenitic steels (concave surface, subscale thickness 30 μm)
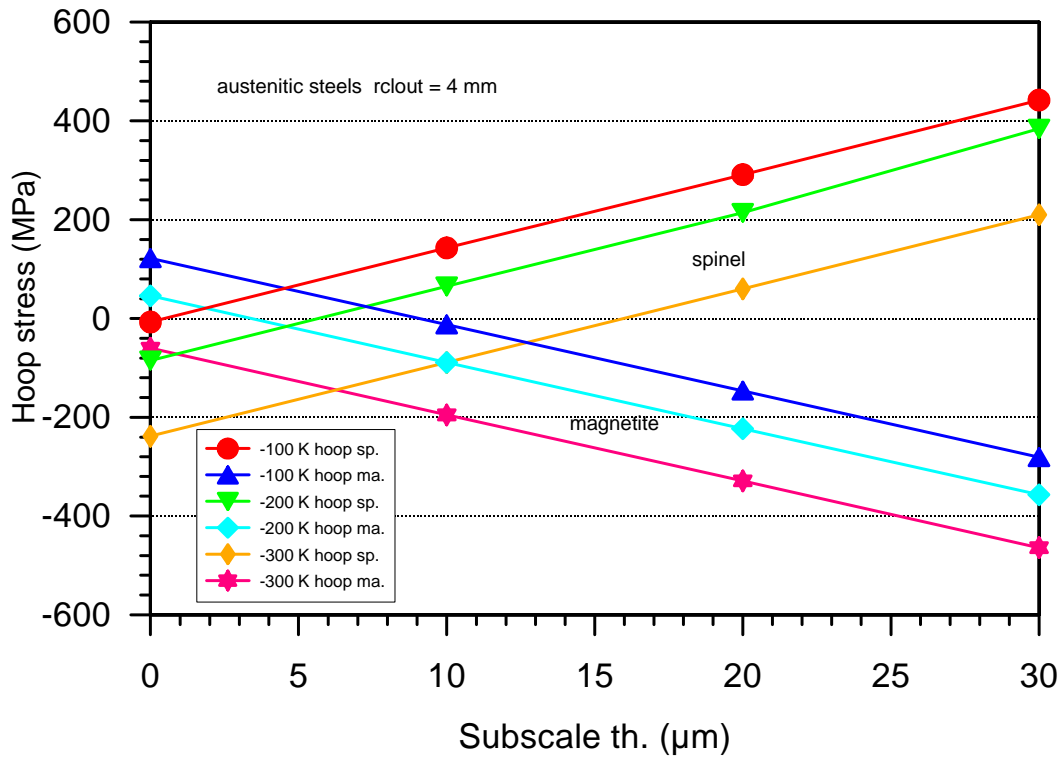
24

Fig. 17 Hoop stresses in the duplex scale on austenitic steels versus the subscale thickness with the temperature ramp as parameter (austenitic steels, convex surface)
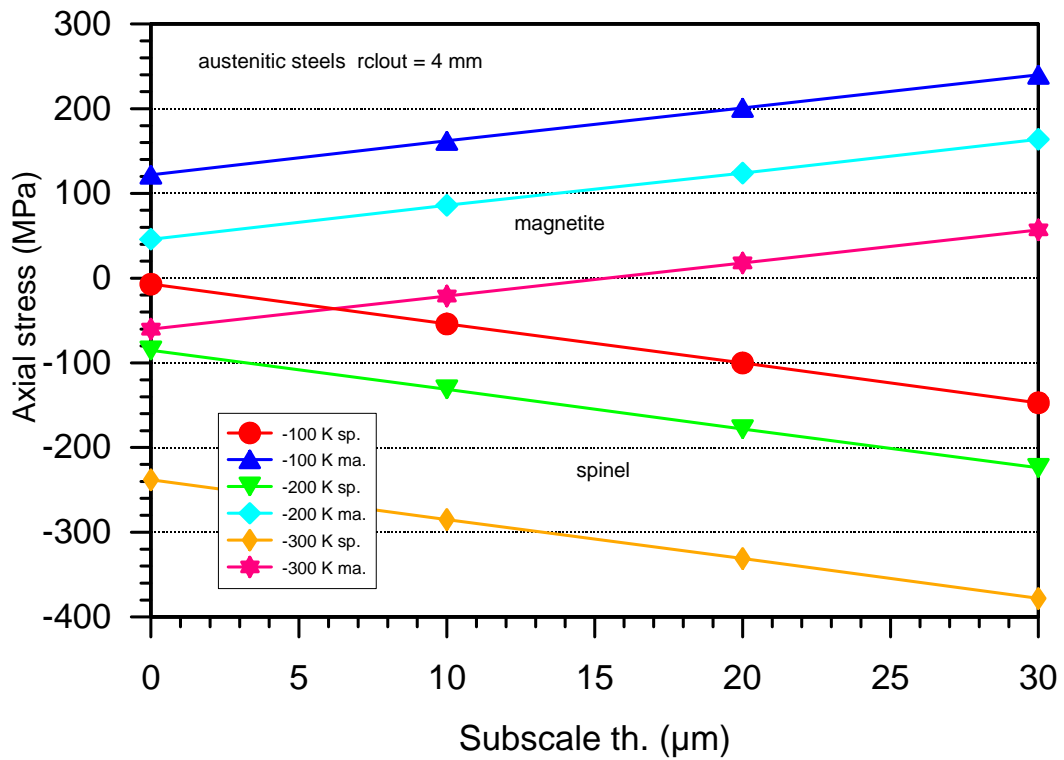


Fig. 18 Axial stresses in the duplex scale on austenitic steels versus the subscale thickness with the temperature ramp as parameter (austenitic steels, convex surface)
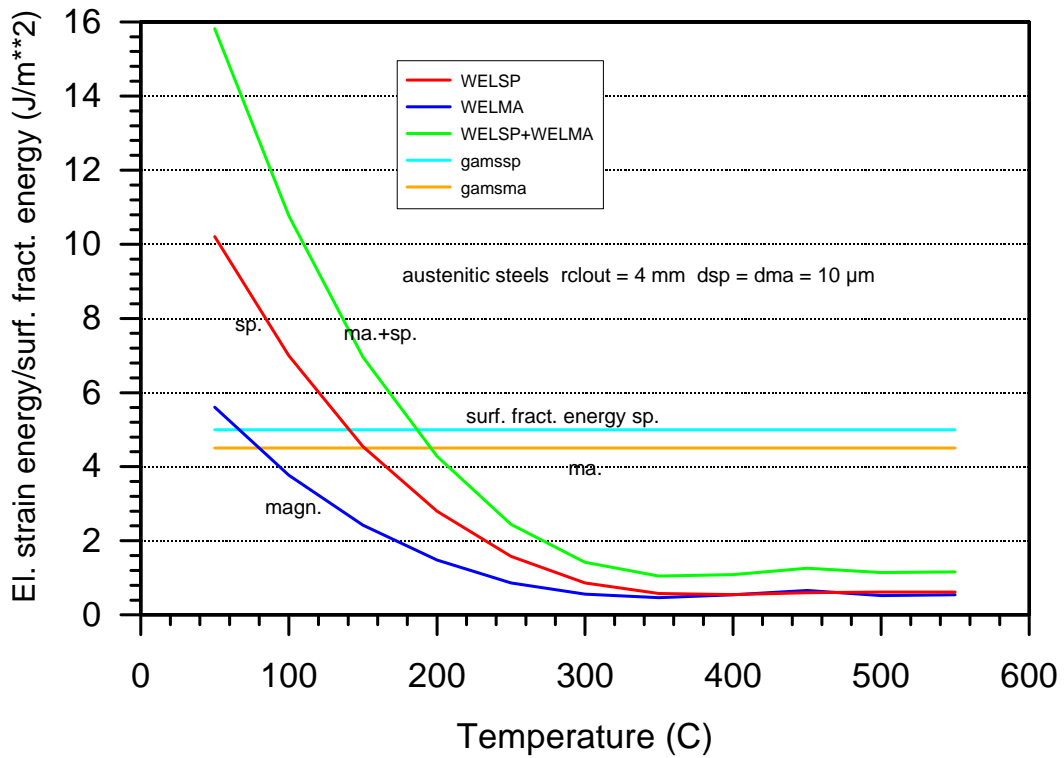
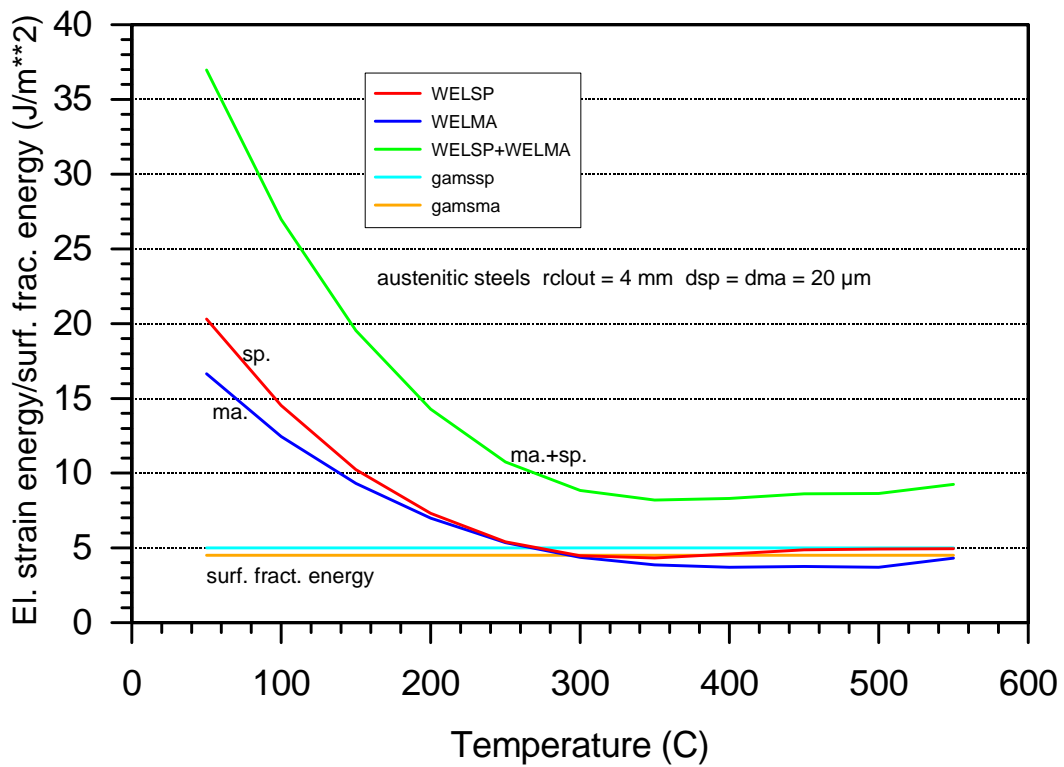Fig. 19 Elastic strain energy in the duplex scale on austenitic steels (convex surface, subscale thickness 10 µm)



Fig. 20 Elastic strain energy in the duplex scale on austenitic steels (convex surface, subscale thickness 20 µm)
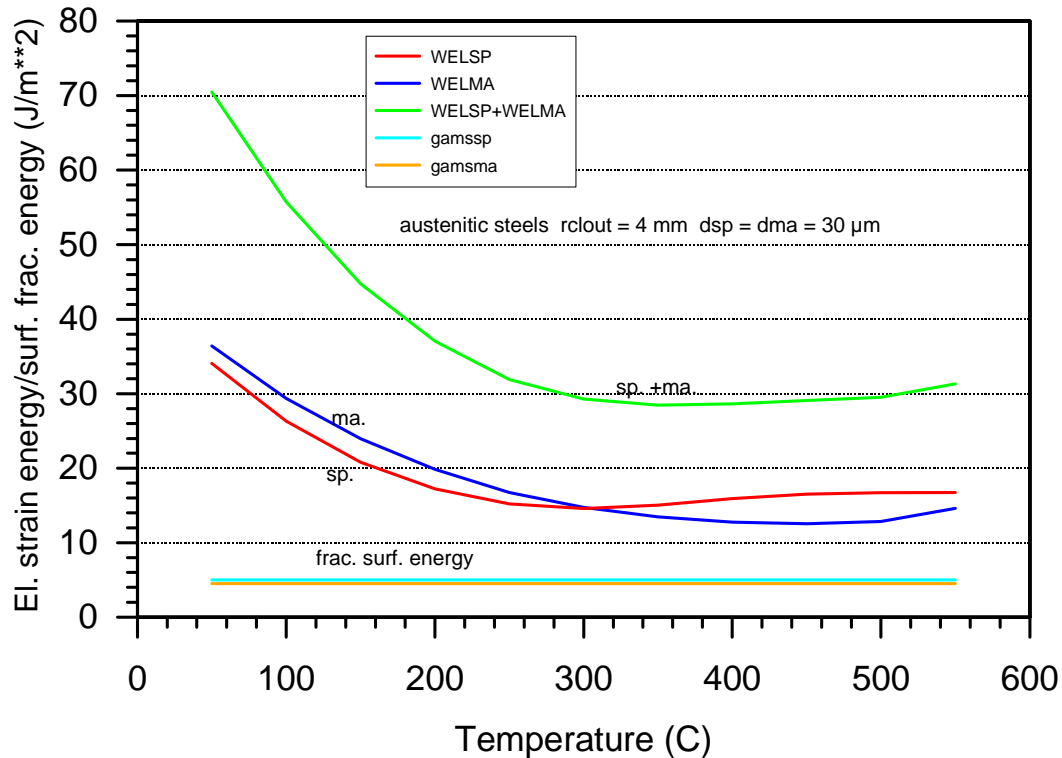
26

Fig. 21 Elastic strain energy in the duplex scale on austenitic steels (convex surface, subscale thickness 30 μm)

# 5.    Experimental observations on failures of iron oxide scales

Experimental observations on failures of iron oxide scales exist for scales grown under gas atmospheres and for scales grown in a heavy liquid metal environment. Although our prime interest is with the case of liquid metal environments, the experience gained from gas atmospheres is also valuable and should therefore not be dismissed.

## 5.1    Oxide scale failure under gas atmospheres

In fig. 4-12 taken from ref. [12] data on spalling of oxide scales on AISI 316 are plotted versus the elastic strain energy, which was determined from the cooling strains and metallographic observations. These data were from superheater and reheater tubes of CEGB coal fired plants. The elastic strain energy was calculated based on model assumptions explained in ref. [12]. Geometrically-induced growth stresses, for example, were not taken into account. As the tubes had rather large diameters, this can be justified. Although the curve in Fig. 4-22 cannot directly be applied to a heavy liquid metal environment, it gives us valuable qualitative information on spalling behaviour of austenitic steels and on the order of magnitude of threshold values for the elastic strain energy.

In ref. [12] a failure map for duplex scales grown on austenitic and ferritic steels was also established. According to this map spalling would occur under tensile and compressive stress conditions with similar failure strains. In ref. [12] is also

mentioned that austenitics spall at the oxide/oxide interface because of the voids there and the irregular metal/oxide interface, whilst ferritics can spall at any interphase or even within a subscale layer. One interesting experimental observation for oxide scales on ferritic steels is also noted in ref. [22], namely that the visually observable spallation is much less marked in cyclic oxidation ($< 1\%$) than in isothermal oxidation ($< 25\%$).
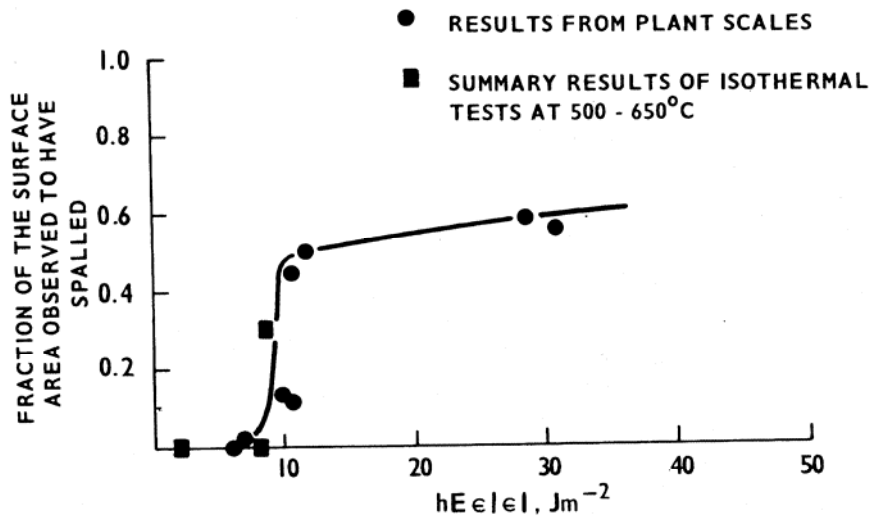


Figure 4-12    Observed Fraction of Spalling as a Function of Stored Energy Function, $hE \in |\in|$, obtained from Metallographic Data

Some examples of mechanical failures of oxide scales on the martensitic steel P92 exposed to steam atmospheres up to 650 $^0$C are shown in ref. [14]. Amongst them are a buckling type failure of the thin outer haematite sublayer, different examples for tensile and shear cracks in the magnetite and spinel sublayers, and decohesion of the spinel sublayer by a wedging mechanism. The buckling and wedging mechanisms and the shear cracks are most probably caused by compressive stresses. This is most clearly shown in fig. 6 of ref. [14] with shear cracks in the spinel layer, decohesion at the interface with the internal oxidation zone and also continuing decohesion at the interface with the magnetite layer. In our opinion the compressive stresses in the spinel layer could only come from intrinsic growth stresses. In ref. [14] are also shown examples for the flakes due to spalling. For oxidation times longer than 500 h these flakes were a mixture of haematite and magnetite.

In ref. [24] it was noted that pitting corrosion followed the loss of the chromic oxide layer due to spalling. It is obvious that the spalling of the oxide scale must have occurred at steady-state conditions.

The stability of isothermally grown oxide scales on ferritic steel was investigated under the conditions of thermal cycling in ref. [25]. It was found that scales formed

upon isothermal oxidation showed locations with bulging behaviour. This is most probably caused by compressive growth stresses and as the test specimens were coupons cut out from strips these must have been intrinsic growth stresses. In response to thermal cycling, the bulging oxide showed poor mechanical stability and continued to crack and spall during each cycle.


## 5.2    Oxide scale failure in heavy liquid metal environments

Oxide scale failure in heavy liquid metal environments can have more serious consequences than the same effect under gas atmospheres, as it may be followed by dissolution of the underlying steel substrate. Dissolution attack of the steel surface has been reported in the literature (see for example [3] and [20]). . This phenomenon is of great technical importance, as it impairs the corrosion resistance of the steel components and one should try to find an explanation for it. In these cases the oxygen concentration in the liquid lead-bismuth eutectic (LBE) was largely sufficient for oxide scale formation, as can be seen by other examples of test specimens One possible scenario could be that there occurred debonding of the oxide scale, filling of the gap between metallic substrate and oxide scale by LBE and then later on spalling of the oxide scale. Why there occurred no renewed oxidation of the steel surface is not yet clear.

In ref. [20] results on martensitic steel specimens in stagnant ant flowing LBE are reported amongst them are interesting examples for mechanical failures of the oxide scales. The martensitic steel Optifer IVc was immersed in stagnant LBE for different test durations at 500 and 550 $^0$C. At 500 $^0$C a single layer oxide scale was formed (presumably Fe/Cr spinel) and at 550 $^0$C a double layer oxide scale (magnetite + Fe/Cr spinel). At 500 $^0$C no oxide scale debonding was observed, whereas at 550 $^0$C there was debonding at the oxide/oxide interface. At the longest test duration the magnetite sublayer has spalled and the spinel sublayer was dissolved to a large extent. This means that the spalling occurred at steady-state most probably due to growth stresses. The debonding of the oxide scale for the test specimens with shorter test durations occurred most probably at the end of the tests upon unloading (downwards temperature ramp).

Debonding at the oxide/oxide interface confirms the experience on duplex scales obtained under gas atmospheres (see for example [12] and [15]). These authors have explained the effect by a reduction of the surface fracture energy caused by the presence of pores at the oxide/oxide interface.

Examples on oxide scale decohesion effects for the martensitic steel T91 exposed to flowing LBE at 550 $^0$C can be found in [21] and [26]. In this case the gap appears at the interface of the spinel subscale and the internal oxidation zone. The gap can be empty or filled with LBE. In the latter case the LBE must have been still liquid, when the debonding event occurred.

Debonding is viewed to be caused by the action of compressive stresses in the oxide scale. But the thermal stresses in oxide scales on martensitic steels are of tensile nature. Therefore it must have been the growth stresses, which induced decohesion and we are inclined to conclude that it occurred atsteady-state. The geometrically-induced growth stresses are compressive in the magnetite subscale and tensile in

the Fe/Cr spinel subscale. The intrinsic growth stresses would be compressive in both subscales. The geometrically-induced part would presumably not be sufficient in view of the low subscale thickness values observed for example in ref. [20] (3 and 6 µm). We had also found indications for the presence of intrinsic growth stresses in the literature (see ref. [4] and [5]).

The question whether scale decohesion for martensitic steels occurs at steady-state or only at the unloading of the test specimens is a very important one, as decohesion might evolve into spalling of the scale and the answer to this question could also provide insight into fundamental aspects of the growth stresses. Experimental evidence can eventually be obtained with the help of microphones installed in the test loops. This technique was, for example, applied in ref. [14], but only during the temperature ramps and not at steady-state conditions.


## 6.    Conclusions

Simple models for the combined effect of thermal and growth stresses in duplex scales on austenitic and martensitic stainless steels have been developed and applied. Of course, there are still open questions like the importance of intrinsic growth stresses, the stresses caused by internal oxidation and the failure criteria for a mixed stress state. Nevertheless, we have gained valuable insight into the problem of mechanical stability of oxide scales grown in heavy liquid metal environments.

The main parameter characterizing the mechanical load of the oxide scales is viewed to be the elastic strain energy. The values of this parameter have been compared to values of the surface fracture energy. In this way a simple criterion for the mechanical failure of the oxide scale was established. It is not yet clear whether such a criterion is fully sufficient, as the hoop stress and the axial stress components can have a different signs. Also, it is not clear whether tensile and compressive stresses can be dealt with the same criterion. It should be kept in mind that mechanical failure of the oxide scale is a stochastic process. A more basic concept of oxide scale failure would consider the growth of cavities. But this was outside our capabilities, as this would need systematic experimental studies on oxide scales.

Systematic studies on mechanical failures of oxide scales grown in gas atmospheres have been done in the past and we can take profit of this work. For oxide scales grown in heavy liquid metal environments we have found some examples for mechanical failures in the literature, but no systematic study of these effects has been done so far. The main question is whether these failures occur predominantly during temperature changes or at steady-state. We have found indications for mechanical failures in oxide scales on martensitic steels caused by compressive stresses. This would then mean that intrinsic growth stresses were active.

## References

[1]     J. R. Nicholls, H.E. Evans and S.R.J. Saunders, Mat. High Temp., 14 (1997) 5-13

[2]     C. Schroer, Z. Voß, O. Wedemeyer, J. Novotny, J. Konys, A. Heinzel, A. Weisenburger, G. Müller, internal report (2005)

[3]     J. Zhang, N. Li, Y. Chen, A.E. Rusanov, Journ. Nucl. Mat. 336 (2005) 1-10

[4]     J. D. Noden, C.J. Knights, and M.W. Thomas, Br. Corr. Journ. 3 (1968) 47-55

[5]     S. Gray, K. Berriche-Bouhanek and H.E. Evans, Mat. Sc. For. 461-464 (2004) 755-761

[6]     H. Steiner report FZKA 6737 (2002)

[7]     M. I. Manning, Corr. Sci. 21 (1981) 301-316

[8]     C. H. Hsueh and A. G. Evans, Journ. Appl. Phys. 54(11) (1983) 6672- 6686

[9]     J. Sung and P. S. Nicholson, J. Am. Cer. Soc. 73 (1990) 639-644

[10]    H. E. Evans, Int. Mat. Rev. 40 (1995) 1-40

[11]    S. Timoshenko: ''Theory of elastic stability'' p 367 McGraw-Hill New York (1936)

[12]    J. Armitt, D.R. Holmes, M.L. Manning, D.B. Meadowcroft, and E. Metcalfe, EPRI Report N4 FP-686 (1978)

[13]    C. Petersen, report KfK 3469 (1983)

[14]    S. Osgerby, Mat. High Temp. 17(2) (2000) 307-310

[15]    J. Robertson, M.I. Manning, Mat. Sc. Technol., 6 (1990) 81-91

[16]    M. Schütze, Ox. Met. 44 (1995) 29-61

[17]    M. M. Nagl and S.R.J. Saunders and V. Guttmann, Mat. High Temp. 12 (1994) 163-177

[18]    H. E. Evans, G.P. Mitchell, R.C. Lobb and D.R.J. Owen, Proc. R. Soc. Lond. A 440 (1993) 1-22

[19]    H. E. Evans, Mat. High Temp. 12 (1994) 219-227

[20]    A. Heinzel, report FZKA 6823 (2003)

[21]    C. Schroer, Z. Voss, O. Wedemeyer, J. Novotny and J. Konys, to be published

[22]    F. Toscan, L. Antoni, M. Dupeux and A. Galerie, Mat. High Temp. 20 (2003) 543-550

[23]    V. K. Tolpygo and D.R. Clarke, Acta mater. 46 (1998) 5153-5166

[24]    H. E. Evans, D.A. Hilton, R.A. Holm, and S.J. Webster, Ox. Met. 14 (1980) 235-247

[25]    R. K. Singh Raman and J.B. Gnanamoorthy, Mat. High Temp. 10 (1992) 171-176

[26]    C. Schroer, private communication

[27]    J.W. Hutchinson and Z. Suo, Adv. Appl. Mech. 29 1992) 63-191

[28]    A. G. Evans and J. W. Hutchinson, Acta met. Mat. 43 (1995) 2507-2530

## Notation

E =     Young's modulus
$\nu$ =     Poison number
$\alpha$ =     lin. thermal exp. coeff.
T =     temperature
$\delta$, s =  thickness
$\sigma$ =     stress
$\varepsilon$ =     strain
W =     elastic strain energy
$\Phi$ =     Pilling-Bedworth ratio
G =     energy release rate
$\Gamma$ =     fracture toughness
K =     stress intensity factor
c =     flaw size
$\gamma$ =     surface energy
G =     elastic energy release upon cracking

## Superscripts and subscripts

ox =    oxide or oxidation
me =   metal
therm. = thermal cycling
r =     radial
$\Theta$ =     azimuthal
z =     axial
ma =   magnetite
sp =    spinel
lay =   layer
av =    average
gr =    growth
i.o.z. = internal ox. zone
f =     fracture
cl =    cladding
o.p. = one particle solution